ETH
Eidgenössische Technische Hochschule Zürich
Swiss Federal Institute of Technology Zurich

ibk

Morena Giulieri

Feasibility study and numerical investigation of novel timber veneer-wrapped steel columns

Master Thesis

Institute of Structural Engineering (IBK)
Swiss Federal Institute of Technology (ETH) Zurich

Supervision

Prof. Dr. Andreas Taras,
Dr. Valentino Vigneri

SS 2023

Abstract

The main focus point of this master thesis is to investigate the behaviour under axial compression of composite columns made with a cylindrical hollow high strength steel profile wrapped around by a beech veneer layer. The wrapping procedure is done by hands with cheap and basic laboratory materials, nevertheless the achieved accuracy in the cross-section is satisfactory. The effect of the column's length is analysed by testing two batches of columns, 28 cm and 2 m high. Moreover, the influence of the inclination's angle of the veneer layer is analysed by building two types of composite column: one with the veneer's fibres orientated along the length of the column and the second with an inclination of 15°. The later proved to be disadvantageous in terms of stability and resistance. The main outcome of this research is that the outer timber veneer layer constrains both local and global buckling of the columns, gaining in term of resistance with an increase in peak force up to 27% compared to the pure steel profile. Additionally, the veneer timber is tested in bending, tension and compression, to get the material properties needed as input into the numerical model in ABAQUS 3D. The developed numerical model manages to predict with a maximum error of 6% the behaviour of the long composite columns under compression.

Acknowledgement

First of all, I would like to sincerely thank my supervisor Dr. Valentino Vigneri for the support during the entire semester. The help during the hard work during the wrapping procedure for the long columns was indispensable to achieve specimens which could be tested without massive imperfections. Moreover, thanks to his experience on using the software ABAQUS 3D I was able to build and validate a model which simulates in an accurate manner the behaviour of the columns. I also want to thank him for taking precious time to discuss the next steps at crucial moments of the research.

I would also like to thank the entire BAUHALLE groups for the valuable advices and technical support during the experimental tests. Without them it would have been impossible to construct and test all the columns and to perform the material tests on the timber specimens.

Last but not least, I would thank Prof. Dr. Andreas Taras for taking the time to propose this very interesting Master Thesis and for the feedback following the midterm and final presentation.

Contents

List of Figures

List of Tables

Nomenclature

Acronyms and Abbreviations

STIMBER-COL	Steel timber veneer columns
TFST	Timber-filled steel tubular
CFRP	Carbon fiber reinforced plastic
STC	Steel-timber composite
LVDT	Linear variable differential transformer
DMS	Dehnungsmessstreifen
DIC	Digital Image Correlation

Introduction

The use of composite section is becoming everyday a more broader approach, this allows to take advantage of the strengths of two different materials and at the same time compensate their weaknesses, building therefore an hybrid material with increased and improved structural properties. Moreover, the increased attention on the topic of sustainable material due to climate change has projected a spotlight on timber as building material due to its lower ecological footprint compared to other conventional construction materials. Therefore, to improve the properties of timber and overcome its weaknesses the combination with other structural materials as concrete and steel has become a frequent practice. Numerous advantages are achieved such as higher load capacity and stiffness, better fire behaviour as well as lower dead weight and smaller cross-section compared to the pure timber section.
Various studies have been done in combining steel and timber, the detailed description is presented in the Literature Review in Chapter 1. The main structural elements built in a composite manner using steel and timber are beams and slabs, less attention has been put on composite columns. To sum up the actual state of the art the main practice is to built columns with hollow steel profile and fill them with timber material. This method is proven to be efficient in constraining local and global buckling of the thin steel profile, resulting in an increase of the overall strength. Only few studies analyse the effect of an outer layer of timber. The importance in further research on such elements is of central importance to advance the composite technology and consequently improving the way columns are built by making them more efficient and at the same time reducing the use of polluting materials. This is the main reason why this thesis focuses on analysing steel-timber composite columns with an outer layer of timber veneer.
The main aim of this master's thesis is to prove that it is possible to hand-build with cheap and basic resources composite columns with beech veneers wrapped around an high strength steel cylindrical hollow profile, that are more efficient than the pure steel profile. This would prove that with adequate funding and the development of a specialised machine, even better results could be achieved than those found during this preliminary study. In parallel, a numerical study is also carried out that can emphasise the simulation potential of the ABAQUS 3D software even with gross simplifications on the behaviour of materials and the experimental test setup.

Chapter 1

Literature Review

The main topic of this master thesis is the construction of composite timber and steel column and its behaviour under axial compression. Various studies in the field of timber and concrete composite system have been done. Already in the 1920s, floors began to be built with wooden planks or boards as support for a concrete deck. This hybrid construction has been further developed and is one of the most used nowadays. A further improvement in the composite floor technology is the replacement of the concrete in the composite steel beams with a timber slabs. This topic is analysed in detail by Hassanieh et al. [1] who studied experimentally the behaviour of a steel I-Profile with an upper timber slab connected via bolts and screws and is proved to be an attractive substitute to the concrete slab in hybrid structures.
In addition to slabs also steel-timber columns have been studied in more recent years, the majority of these studies focus on timber-infilled steel profiles. Qiao et al. [2] experimentally studied the behaviour of stub columns under axial compression, these columns are constructed with square steel tube filled with timber reinforced with carbon fiber reinforced plastic (CFRP), the later provides confinement and the results show an increased strength and ductility compared to the pure steel or timber columns. Moreover, the hybrid member shows a better weight-strength ratio. It is also highlighted that the presence of knots and imperfections in the timber member have a relevant effect on the stability. A similar study is proposed by Karampour et al. [3] who implemented a new fabrication procedure for timber-filled steel tubular (TFST) columns, which does not need glue or mechanical connectors. These columns are constructed with a SHS steel profile and four pieces of radiata pine timber. From the experimental and analytical analysis results that the TFST columns have increased compression strength in fibre direction, which puts this product at the same level of concrete-filled steel tubular columns but with the advantage of the lighter composition. Cylindrical steel cross section has analysed too by Ghazijahani et al. [4]. The steel profile is filled with solid timber and confined by CFRP. The composite columns show improved capacity under axial compression and the benefit of a lighter structure compared to concrete-filled columns. Ghazijahani et al. [5] went even further by combining three materials and analysing the behaviour of innovative double-skin concrete-timber-filled steel columns under compression. The specimens constructed with an hollow square steel profile filled with concrete and with various layout of reinforcement steel bars and secondary hollow steel profile filled with timber.

Less attention has been put on the analysis of steel-timber columns with inner steel profile and an exterior layer of timber. Only two recent researches investigated such topic, the first is an experimental study done by Hu et al. [6] on a steel HEA profile wrapped by a glulam and the second examines a composite column with the steel profile encased into the timber by Kia and Valipour [7].
The schematic representation of the cross section analysed in the first research is shown in Figure 1.1. The exterior timber layer is applied with and adhesive and is proven to provide confinement to the steel profile against buckling, being therefore beneficial in term of stability. In this study the behaviour of the column under axial compression is analysed. Three lengths are tested, namely 1100,

1700 and 2300 mm as well as three combinations i.e. steel-timber composite (STC), only timber and only steel. For the hybrid column the HEA profile with strength class Q235B is selected and the glulam made of first grade Douglas-fir is bonded to the steel with a mixed structural-epoxy adhesive. Lateral deflection and axial displacement are measured by linear variable differential transformers (LDVTs).

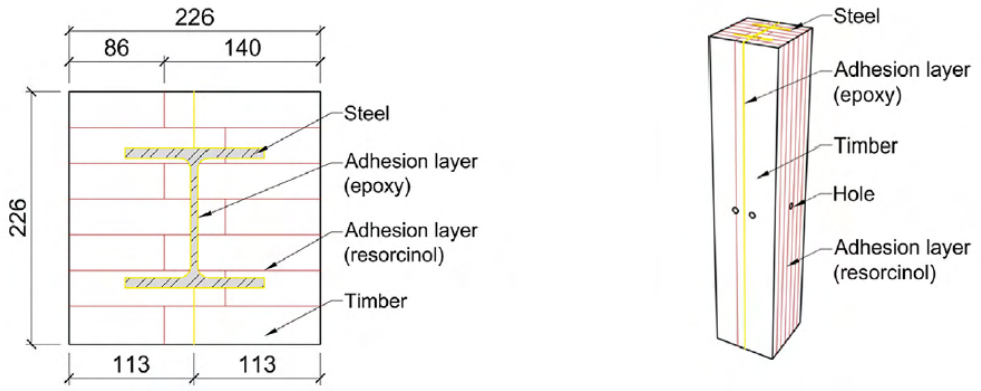

Figure 1.1: Cross section and view of STC column by [6]

The results shown as load - displacement curves in Figure 1.2, 1.3 and 1.4, respectively for the columns 1100, 1700 and 2300 mm long, highlight three main phases. The first is the elastic phase with a poor activation of the interaction mechanism between steel and timber, while in the following yield phase the outer timber layer provided confinement against the overall and local buckling of the interior steel profile. Lastly during the residual load-carrying capacity phase the length of the columns played a role in terms of ductility, in fact was determined by the steel for the smaller specimen and by the timber for the longer one. The comparison between lengths shows that the maximum ultimate lateral deflection increases with the length, while the initial stiffness and the maximum load decrease. This can be explained by the size effect, with larger specimens is more likely to have imperfection in the material, which can lead to lower structural properties. Two main failure modes for the composite columns are found, a strength failure occurred for the shorter columns while for the columns 1700 mm and 2300 mm long an overall instability along the weak axis of the steel profile arose. The beneficial effect of the composite profile is clearly visible in all figures, since the black lines, that show the behaviour of the STC, reach always higher values compared to the dotted and the dashed lines, which respectively represent the bare timber and steel profile.
To discuss the results in terms of superposition of single material and composite profile the Figure 1.5 shows a histogram which compares the maximum load, cross-section area and average strength of STC, timber, steel and the superposition the latter. The maximal load of the STC is slightly lower than the superposition of timber and steel contrary to the average strength which is higher for the STC. This underline the possible benefit of this technology and in addition there is a clear advantage in the reduction of the cross section with the composite profile compared to the superposition. Further study in this sense should be done to prove that the superposition of single material such as timber and steel are less efficient than the hybrid column.

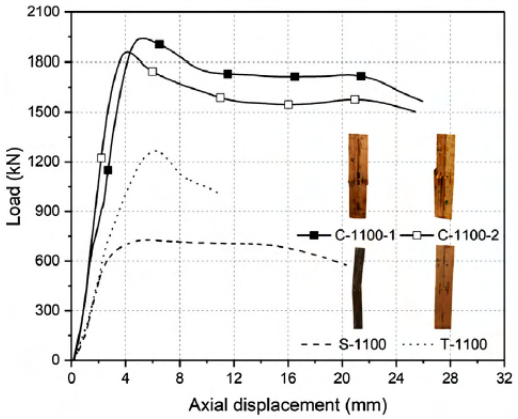

Figure 1.2: Load curve specimen 1100 mm long by Hu et al. [6]

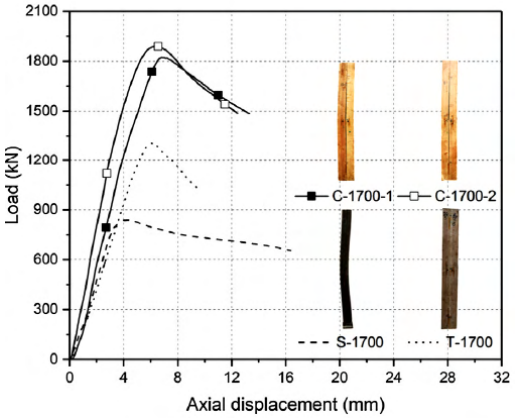

Figure 1.3: Load curve specimen 1700 mm long by Hu et al. [6]

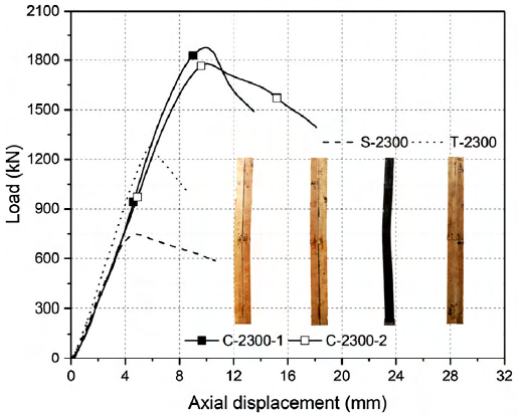

Figure 1.4: Load curve specimen 2300 mm long by Hu et al. [6]

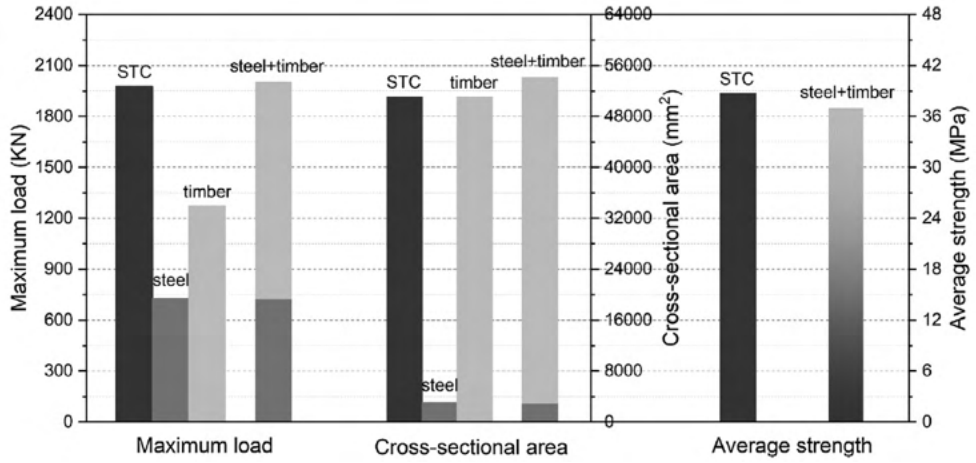

Figure 1.5: Schematic comparison of maximum load, cross-section area and average strength by Hu et al. [6]

The second study of Kia and Valipour [7] focus on a timber-steel composite columns but the idea is to reinforce the timber with a solid steel bar as core. All columns are tested in compression and various parameters are investigated as column's length, reinforcement's geometry, type of timber, steel and timber grade. In Figure 1.6 are shown some of the different layout investigated in the study as a bare timber cross section, a composite column with a square reinforcement with yield strength of 300 MPa and a second composite one with a round bar with an higher yield strength of 420 MPa. The abbreviations used are the following:

- Timber type: P = Pine or D = Douglas fir
- Length: 0.9 m or 1.2 m
- Reinforcement geometry: bare timber profile, S = square or R = round
- Size of reinforcement: 16 or 20 mm
- Yield strength: 300, 420 or 660 MPa
- Application interface of epoxy adhesive:
  - CA = between two timber pieces
  - CO = around steel profile
  - CC = both

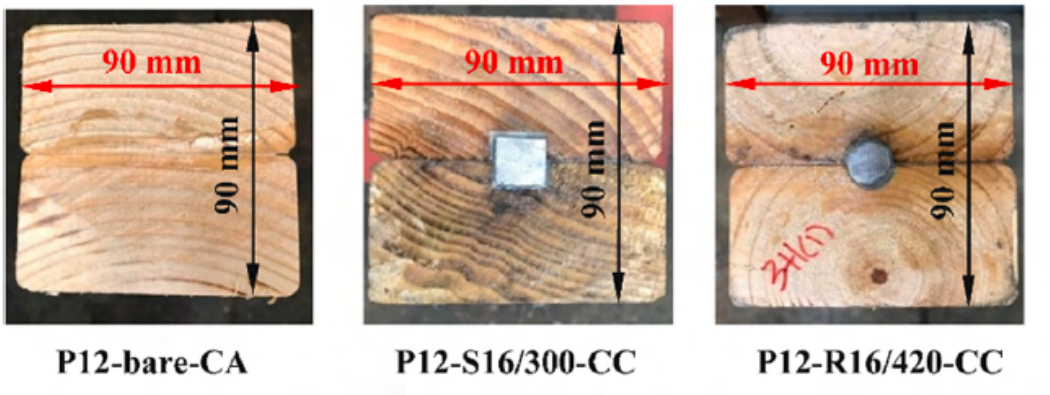

Figure 1.6: Cross section of encased steel-timber columns by [7]

The results of the axial compression are summarised in Figure 1.7 as mean load-displacement curves over all specimens. The main failure mechanism results from the combination of buckling of the steel profile induced by second order effects and timber crushing. As visible in the graphs below the black solid curves, representing the bare timber profiles, have always a smaller ultimate compression strength compared to the composite timber steel columns. It is also highlighted that with bigger reinforcement's cross-section and maintaining the same steel and timber grade there is an increase in strength but a lost in term of ductility. Also by increasing the yield strength the load carrying capacity is improved. Moreover the experimental stiffness of the columns is smaller than the theoretical one, this is mainly due to knots and imperfections present in the timber which highly reduce the actual elastic modulus. Their presence not only influence the stiffness but also the ultimate load carrying capacity as well as the failure mechanism in particular when are situated in the middle of the columns.
As conclusion there are multiple benefits in the use of encased steel reinforcements into timber casing such as reduction of the cross section of the structural member compare to bare timber, fire protection for the inner steel reinforcement, lighter structure with higher strength/weight ratio and lower cost by using cheaper low-grade timber such as pine and douglas.

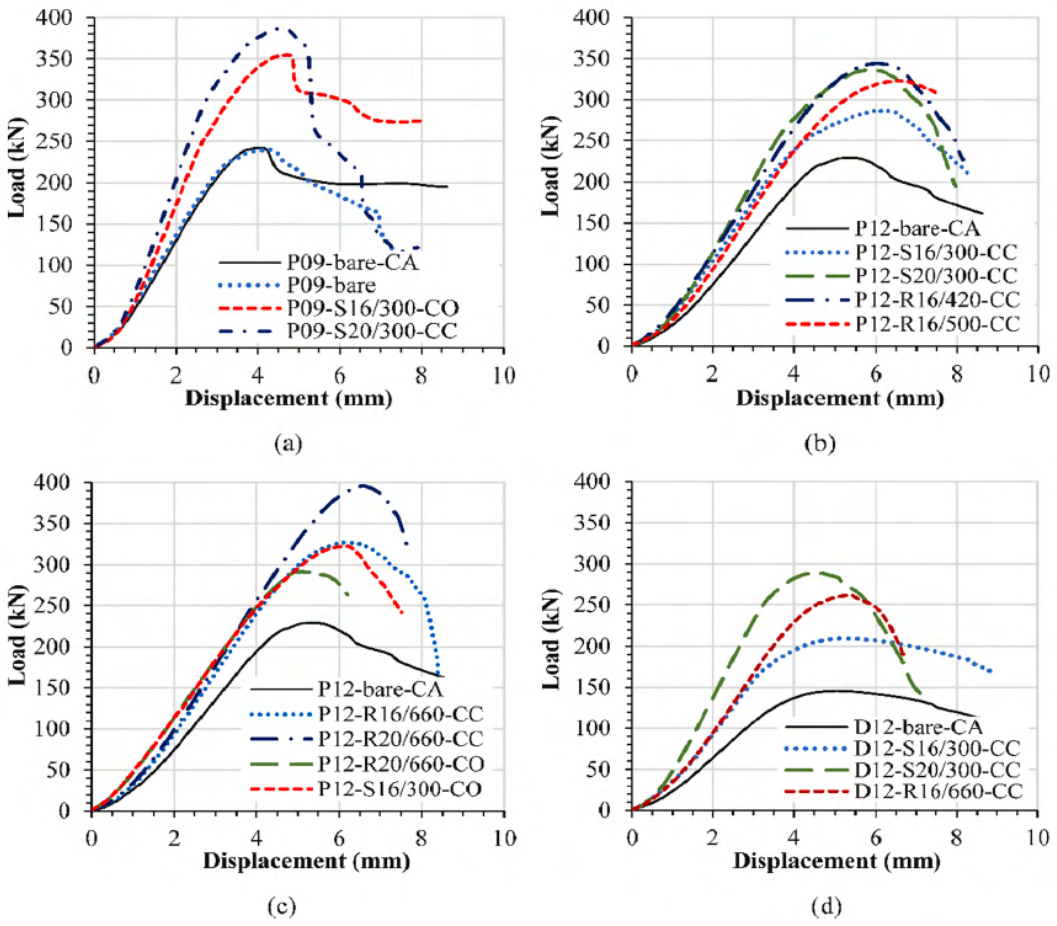

Figure 1.7: Mean load-displacement curves of bare timber and composite columns by [7]

Chapter 2

Materials and Methods

In this section the construction of the specimens, the setup as well as the procedure for the tests are described in detail. Three category of specimens are built, one for each test performed, namely the four point bending and tensile tests and the axial compression test. The furthers are performed to find the material properties of the timber veneer layer and the later to investigate the behaviour of the composite columns under axial compression. The materials used for the construction of the specimens are summarised in Table 2.1.

Table 2.1: Material list

Component	**Type**	**Dimensions**
Steel columns	Steel grade S355 see Appendix A	D_e = 82.50 mm Thickness = 3.60 mm
Glue	LOCTITE HB S309 Purbond see Appendix B LOCTITE HB S709 Purbond	Thickness $\cong$ 0.10 mm
Timber veneer	Beechwood	Thickness = 0.60 mm

2.1 Material tests

The material tests done to define the material properties of the timber veneer layer around the steel profile are the four point bending and the tensile test. The same material as for the columns is used to built the specimens. In the following subsection the construction method and the test procedure are described.

2.1.1 Timber specimen construction

Two batches of timber veneer are used for the construction of the columns, one for each type of columns. From the timber veneer of the first batch (S - Stub) a plate is built with twelve layers glued together, while for the second batch (L -Long) the plate is composed by fifteen layers; from those plates the specimens for the two tests are cut. The procedure for the construction of the plates is the following:

1. The long timber veneers are cut with a width of 50 cm and a length of 80 cm
2. Over each layer the glue is evenly spread as shown in Figure 2.1
3. The plate is compressed with two rigid planks as shown in Figure 2.2
4. The samples are stored in the clima-box at constant air temperature of ca. 18.8 °C and relative humidity of ca. 54.2% for 12 hour for hardening

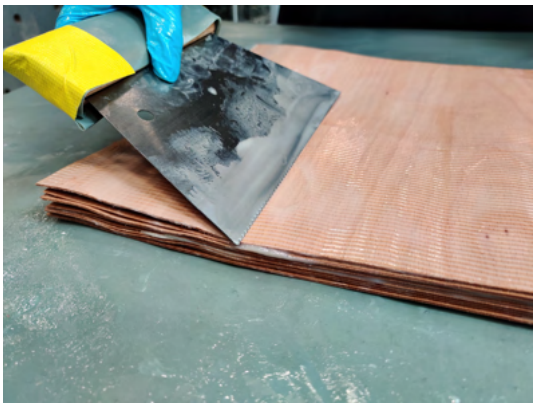

Figure 2.1: Application of glue on the veneer

Figure 2.2: Compression of timber veneer plate

2.1.2 Four-point bending test

The specimens for the four point bending test have a rectangular shape, the dimensions are defined according to the requirement of Euro Norm EN408 [8]. The overall thickness is of ca. 9 mm, the length between the two loading points is defined as six times the thickness and is therefore of ca. 54 mm, the distance between the supports is defined as $L = 18 \cdot t \pm 3 \cdot t$ is then chosen to be 162 mm while the width is freely chosen as 20 mm. The overall length of the sample is of 240 mm with additional length of 39 mm on both sides as shown in Figure 2.3. A total of ten specimens per batch are tested, they are further divided into two subcategory which differ in the orientation of the timber veneer fibres, one longitudinal and one perpendicular to the timber fibres as shown in Figure 2.4. Five specimens for each orientation are tested. In Appendix C are summarised the measured dimensions for each sample, the abbreviation used for simplicity define first the type of test "B" for bending, then the batch "S" for stub columns or "L" for long and the number indicate the inclination of the fibres "0" for the longitudinal and "90" for the perpendicular.

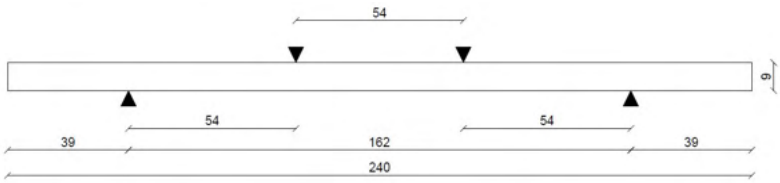

Figure 2.3: Specimen geometry for four point bending test

Figure 2.4: Four point bending specimens

The ZWICK retro 10/200 kN machine is used for the four point bending test and the setup is visible in Figure 2.5. The test is performed in displacement controlled mode, a pre-load of 10 N is applied with a speed of 50 mm/min afterwards the speed is decreased to 1.2 mm/min and the test is stopped when a drop of 25% in the maximum force is reached.

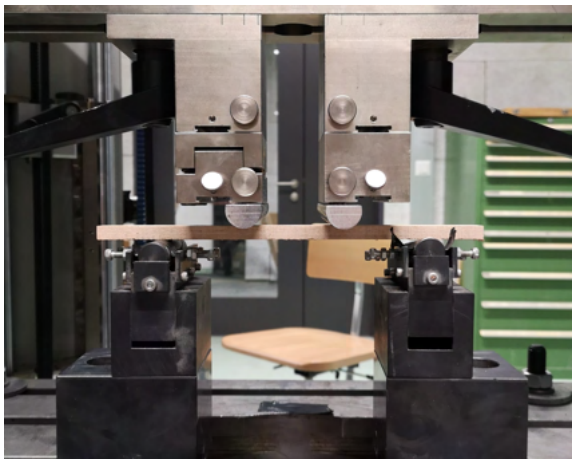

Figure 2.5: Setup four-point bending test

The variables measured during the test are the force and the displacement of the cross head, the later is assumed to be equal to the deformation of the specimen since the components of the setup are way stiffer compared to the sample. From the maximum force and the geometry of the specimen is possible to extrapolate the bending strength of the timber veneer longitudinal and perpendicular to the fibres with the Formula 2.1 from the Eurocode DIN EN 408 [8]. The parameter a is the distance between the support and the loading point, b and h are respectively the width and the thickness of the specimen.

$$f_{m,\phi} = \frac{3 \cdot F_{max} \cdot a}{b \cdot h^2} \tag{2.1}$$

Moreover the stiffness of the specimen is computed with the Formula 2.2 from the Table C4 [9] for the same setup as the test, with the parameter $\alpha = a/l$ and l the distance between the two base supports and with w as the deformation in the middle of the specimen.

$$E_{m,\phi} I \cdot w = \frac{1}{24} \cdot F_{max} \cdot l^3 \cdot (3\alpha - 4\alpha^3) \tag{2.2}$$

2.1.3 Tensile test

The second material test performed is the tensile test. The specimens are cut off the same plate as for the bending test. The samples have a bone shaped geometry, thereby the failure will occur in the middle where the width of samples is smaller. The geometry is shown in Figure 2.6. The thickness as before is of ca. 9 mm and according to the Euro Norm EN408 [8] the length should be ten times the thickness. Therefore, the part between the two grips is set to 90 mm, the width inside the grips is freely chose as 2.5 cm. Three orientations of the timber veneer fibres are analysed: longitudinal, with 15° inclination and perpendicular. A total of fourteen samples pro batch are tested, five for the first two category and four for the third one. In Figure 2.7 are shown all specimens tested. In Appendix D are summarised the measurements of thickness, width and length for each sample, the abbreviation used are the same as for the bending test but with "T" for tensile and in addition there is the inclination in degrees of "15".

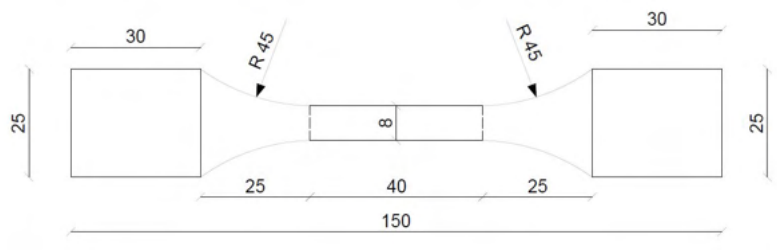

Figure 2.6: Specimen geometry for tensile test

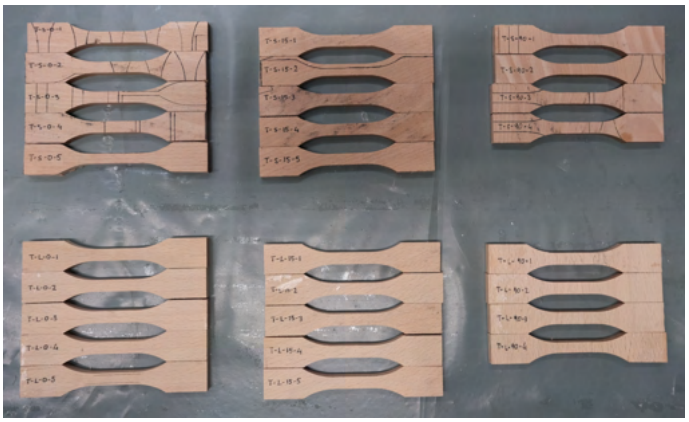

Figure 2.7: Tensile specimens

The ZWICK retro 10/200 kN machine is used, the setup for the test is shown in Figure 2.8. The sample is placed in the middle of the two grips, an extensometer is then attached at the side of the tighter part of the specimen to get the strain during the test. The test is performed in displacement controlled mode, a pre-load of 50 N is applied afterwards the test speed is decreased to 0.2 mm/min. The test for the perpendicular and diagonal specimens is stopped when the samples broke. For the longitudinal one was not always possible to reach the breaking point, because sometimes the sample slipped from the grips and by increasing the constraining force a premature rupture of the specimens was induced. So when the slip occurred the test was ended, the strength computed from the maximum force is therefore only a lower boundary value.

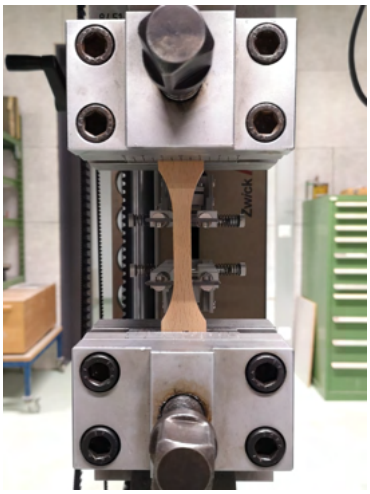

Figure 2.8: Setup tensile test

The parameters analysed are the force applied, the displacement of the cross-head and the strains from the extensometer. The tensile strength is computed with the Equation 2.3 according to the Euro Norm EN 408 [8] where F_{max} is the maximum tensile force reached and A is the cross section area of the specimen. The tensile stiffness is computed with the strain measured and the stress computed from the force with the Equation 2.4.

$$f_{t,\phi} = \frac{F_{max}}{A} \tag{2.3}$$

$$E_{t,\phi} = \frac{\Delta F/A}{\Delta \varepsilon} \tag{2.4}$$

2.2 Column test

In this section the main features of the composite columns are highlighted with the focus on the construction method and the setup of the axial compression test.

2.2.1 Composite columns construction

The composite steel timber veneer columns constructed differentiate from each other for the layout of the outer timber layer as well as the length. In Figure 2.9 is shown a schematic representation of the different type of columns. The first distinction is the length the ones ca. 28 cm long are called "Stub columns" (S) while the ones 2 m long are labelled as "Long columns" (L). Then there is the division in terms of material composition, first there are the composite columns (ST-Steel Timber) then the pure steel profile (S) and for the stub columns there is an additional category namely the pure timber one (T). The final subdivision is defined by the layout of the timber veneer fibre inclinations. The first has the fibres oriented along the axis of the column (0) whereas the second has an inclination of 15° respect to the main axis (15). For the later the veneer orientation is changed four times during the rolling procedure in order to have the same properties in both directions. For the shorter columns five samples are built while for the long columns only three. In Table 2.2 are summarised all the mentioned samples produced with the description of the composition and their abbreviations, which will be used for simplicity.

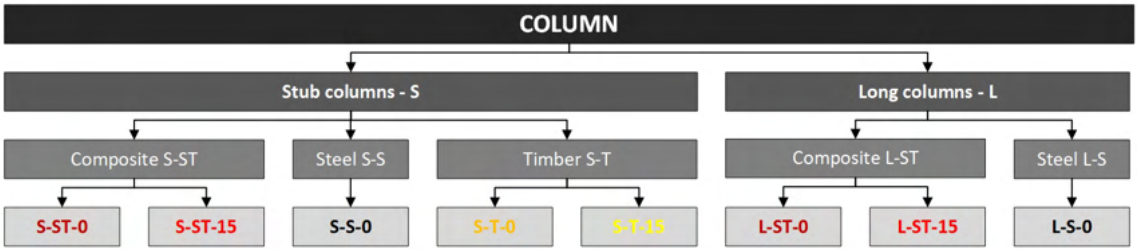

Figure 2.9: Overview columns

Table 2.2: Column sample abbreviations

Stub columns name	**Long columns name**	**Composition**
S-S-0	L-S-0	Steel profile
S-ST-0	L-ST-0	Steel-Timber composite with fibres inclination 0°
S-ST-15	L-ST-15	Steel-Timber composite with fibres inclination 15°
S-T-0	-	Timber profile with fibres inclination 0°
S-T-15	-	Timber profile with fibres inclination 15°

The construction procedure for both stub and long columns is composed by five main steps:

1. The cylindrical steel profile is cut to the desired length (only for the stub columns) and the edges are polished as well as the surface as shown in Figure 2.10.
2. The long timber veneers are also cut to fit the steel profile as shown in Figure 2.11, these smaller pieces are then connected to each other to build a longer roll with a special tape for timber visible in Figure 2.12. To build the columns with the timber fibres inclined by an angle of ca. 15° the veneer pieces are cut with the same angle and inclined connected to each other as visible in Figure 2.13.
3. The glue is evenly spread over the timber veneer roll with a thickness of more or less 0.1 mm, at this point the steel profile is rolled over the veneers and connected until the desired thickness of the timber is achieved, namely 11 - 12 mm which corresponds to ca. twelve layers of veneer. Two types of glue are used, for the stub columns the LOCTITE HB S309, which has a work-time of 30 minutes, while the LOCTITE HB S709 is used for the long columns with a work-time of 70 minutes.
4. Subsequently an aluminium sheet (for the long columns two one meter long sheets are used), previously bent to fit as precisely as possible the column, is placed around the sample and then put under pressure thanks to hose clamps fixed and tighted around the aluminium cylinder as shown in Figure 2.14 and 2.15.
5. The sample is put in the clima-box in an ambient with ca. 18.8°C air temperature and 54.2% relative humidity for minimum two respectively twelve hours for stub and long columns to let the glue harden.

Due to inaccuracy during the rolling of the veneer timber and the in-homogeneity of the timber surface, the aluminium cylinder can not fit perfectly the sample as visible in Figure 2.16. This gap causes an inevitable imperfection along the samples as shown in the cross section in Figure 2.17 along the entire column.

Figure 2.10: Cut steel profile

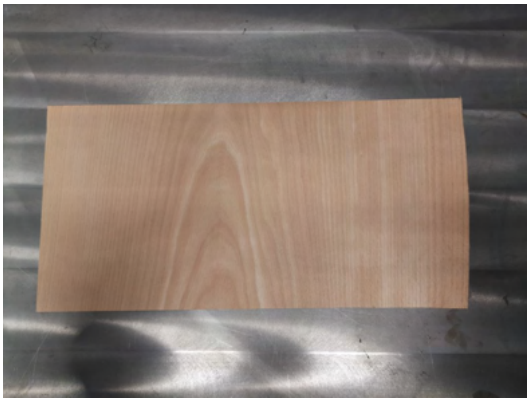

Figure 2.11: Cut timber veneer

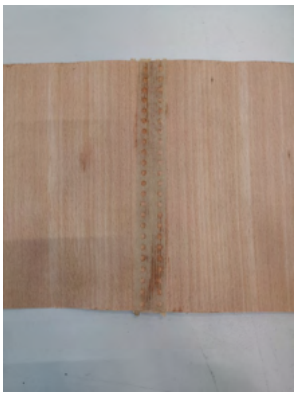

Figure 2.12: Connection timber veneer

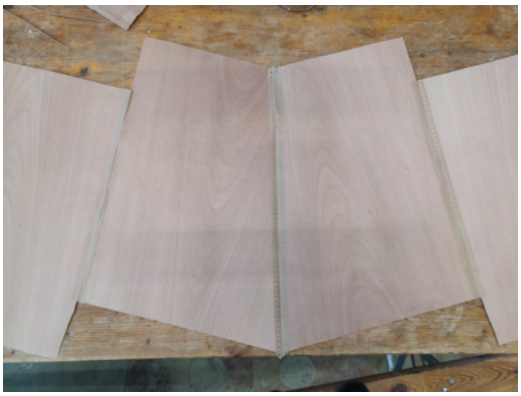

Figure 2.13: Connection of inclined veneer

Figure 2.14: Stub column under pressure

Figure 2.15: Long column under pressure

Figure 2.16: Detail end aluminium cylinder

In Table 2.3 are summarised all relevant dimensions for stub and long columns, namely the inner diameter D_i, the thickness of the steel and timber layers t_{steel} and t_{veneer}, the outer diameter D_o and the cross-section area A_{CS}. For the values related to the timber layer the mean values are reported with the standard deviations. As visible from the values of the standard deviation the longer columns present an higher variability, this is due to the imperfection in the veneer itself and in the construction procedure which was challenging due to the length of the columns. In Appendix E are summarised the measurements of the thickness, diameter and length for each column. From Figure 2.23 to Figure 2.20 are shown the views and cross sections of all stub columns and from Figure 2.27 to Figure 2.26 the one for the long columns.

Table 2.3: Column's dimensions

Sample	$\mathbf{D}_i$ **[mm]**	$\mathbf{t}_{steel}$ **[mm]**	$\mathbf{t}_{veneer}$ **[mm]**	$\mathbf{D}_o$ **[mm]**	$\mathbf{A}_{CS}$ **[mm^2]**
S-S-0	75.3	3.60	-	82.50	892.3
S-ST-0	75.3	3.60	10.71 ± 0.27	103.92	4029.3
S-ST-15	75.3	3.60	12.30 ± 0.76	107.10	4555.6
S-T-0	83.70 ± 0.25	-	10.18 ± 0.44	102.86	2802.5
S-T-15	84.10 ± 0.35	-	10.28 ± 0.55	103.06	2785.4
L-S-0	75.3	3.60	-	82.50	892.3
L-ST-0	75.3	3.60	10.63 ± 1.74	103.76	3919.9
L-ST-15	75.3	3.60	11.20 ± 1.65	104.90	4105.9

Figure 2.17: Cross section S-ST-0

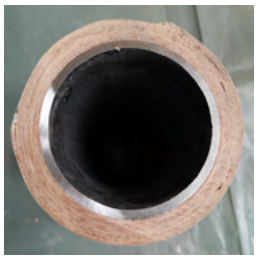

Figure 2.18: Cross section S-ST-15

Figure 2.19: Cross section S-T-0

Figure 2.20: Cross section S-T-15

Figure 2.21: View S-ST-0

Figure 2.22: View S-ST-15

Figure 2.23: View S-T-0

Figure 2.24: View S-T-15

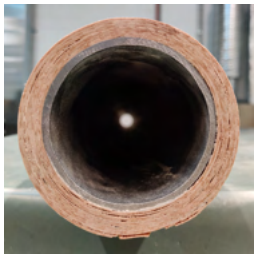

Figure 2.25: Cross section L-ST-0

Figure 2.26: Cross section L-ST-15

Figure 2.27: View L-ST-0

Figure 2.28: View L-ST-15

An additional treatment is done for the long columns, during the axial compression test are used two DIC cameras, which take a picture of the central part of the specimens each second and by post-processing the data a deformation field can be obtained. According to the guideline of this device enough contrast should be ensured to be able to have accurate results. Therefore, the central part of the long columns is painted in white and then black dots are spread over it to get the needed contrast. The size of this dots is defined in the DIC guideline and the formula is reported bellow, where AOI stands for Area of Interest. The painted surface is shown in Figure 2.29.

$$speckle\ size\ [mm] = \frac{AOI\ size\ [mm]}{resolution\ [px]} \cdot 5\ [px] = \frac{500}{4096} \cdot 5 = 0.61\ mm$$

Figure 2.29: DIC surface L-S-0

2.2.2 Axial compression test

The stubs and long columns are tested under axial compression with the Schenck Hydropuls 1600 kN testing machine. For the top and bottom hinge the same set up is used, in Figure 2.30 is shown the bottom convex part which is coated with Teflon and grease to allow a smoother rotation of the top spherical part showed in Figure 2.31. In Figure 2.32 is shown the assembled hinge. This should allows rotation in all directions and constrains all displacements except for the vertical one.

Figure 2.30: Bottom part of hinge

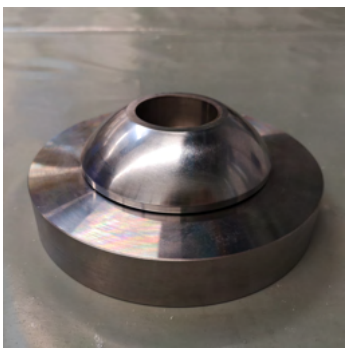

Figure 2.31: Top spherical part of hinge

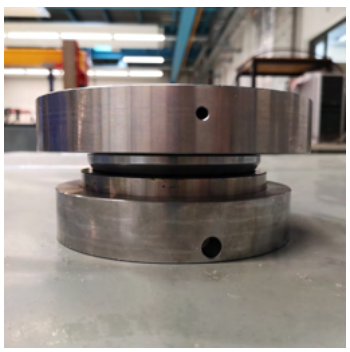

Figure 2.32: Assembled hinge

In Figure 2.33 is shown the complete setup for the stub columns. The two hinges are fixed above and below the specimen, to make sure that the sample is placed in the middle a special whaser is inserted on the top and bottom plate, this piece fits almost perfectly the inner diameter of the steel profile. In Figure 2.33 are also visible the devices used to measure the displacements and the strains in the specimen. Three vertical LVDTs are used and placed around the sample with a spacing of ca. 120° between each other to measure the vertical displacements. They are directly attached to the last steel plates right above and below the specimen to get a more precise measure without taking into account the deformations of all hinge's components. Moreover, three strain gauges (DMS), shown in Figure 2.34, are glued to the inner surface of the steel specimens at an height of ca. 10 cm from the bottom edge with the same spacing as the LVDTs. The setup is the same for all stub columns except for the timber columns which do not have any DMSs.
The test is carried out as displacement controlled, at first the cross head is lowered until the force reaches ca. 1 kN, this is done to ensure that all the pieces of the hinges are in contact before starting the actual test. Initially the speed of the compression is set to 0.1 mm/min and then increased to 0.2 mm/min, once the plastic phase is reached the speed is further increased to 1 mm/min. After reaching the maximum and experience a drop in the force of ca. 25% of the maximum force the machine is stopped and then the unloading procedure is performed with a speed of 0.5 mm/min.

Figure 2.33: Setup of S-S-0

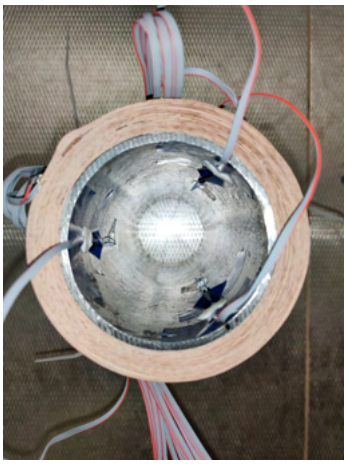

Figure 2.34: DMS-placement in S-ST-0

From the measurement devices the parameters recorded during the test are the force applied, the strains and displacement. From each force-displacement curve is possible to get two main parameters, the maximum force and the stiffness. The later is computed with Equation 2.5, where the strains are either computed with the displacement's measurement of the LVDTs or with the strain's measurement of the DMSs.

$$E = \frac{\Delta F}{A_{CS} \cdot \Delta \varepsilon} \tag{2.5}$$

The axial compression strength along the timber veneer fibres and with and inclination of 15° is computed with the maximum force from the test of the timber samples (S-T-0 and S-T-15) with the Equation 2.6. The cross section area (A_{CS}) is reported in Table 2.3.

$$f_{c,\phi} = \frac{F_{max}}{A_{CS}} \tag{2.6}$$

The set-up for the long columns is similar to the one for the stub columns, the hinges used are the same and the complete setup is shown in Figure 2.35. The vertical LVDTs are attached as before to the plates directly below and above the specimen as shown in Figure 2.36, in addition three horizontal LVDTs, visible in Figure 2.37, are placed in the middle of the column with a spacing of ca. 120°. Moreover, two DIC cameras are used to catch the deformations and the strains of the

painted middle part of the columns. A picture for each second is taken, from which a deformation field can be extrapolated. The same procedure and speed are used as for the stub columns. The test is performed in displacement controlled mode, at first an initial load of 1 kN is applied to make sure that all components are in contact. At the beginning of the actual test the loading velocity is set to 0.1 mm/min and further increased to 0.2 mm/min once all measurement devices started recording. The test is stopped once the force drop to 75% of the maximum load reached.
The same main parameters are computed as for the stub columns, namely the maximum force and the elastic modulus. The later is computed as before with the Equation 2.5.

Figure 2.35: Setup L-ST-15

Figure 2.36: Position vertical LVDT

Figure 2.37: Position horizontal LVDT

2.3 ABAQUS model

In parallel to the physical axial compression tests of the STIMBER columns a finite element model is built to reproduce the structural behaviour of the specimens. This numerical analysis is done with the software ABAQUS 3D, in the following subsections the model is described in detail focusing on the assumptions made and the solving procedure.

2.3.1 Modelling assumption

A representative numerical model of each column is built using the actual dimensions of the specimens, for the thickness of the timber layer the mean values summarised in Table 2.3 are used. Each 3D non-linear finite element numerical model is composed by two main parts:

1. The steel profile is modelled with a 4-node shell elements with reduced integration (S4R), shown in blue in Figure 2.38. This type of element is proven to be adequate for modelling hollow cylindrical steel profile according to the research of Meng and Gardner [10].

2. The timber veneer layer is modelled with three dimensional 8-node solid elements with reduced integration (C3D8R), shown in orange in Figure 2.38.

The timber veneer layer is partitioned into four to model the change in the direction of the veneer fibres done during the construction of the specimens. At first a local cylindrical coordinate system is defined, then for each partition the orientation of the material properties is defined referring to the later. Afterwards the longitudinal direction is inclined by an angle of $\phi = 15°$ alternating the sign for each partition, meaning that the first and third layer have the same inclination and the second and fourth one as well but with opposite sign. In Figure 2.39 is shown the inclination of the outer layer with the following main directions:

1. Radial out-of-plane of timber layer (R)
2. Perpendicular to the fibre (T)
3. Longitudinal to the fibre (L)

The mesh size is defined thanks to the formula $0.5 \cdot \sqrt{D \cdot t}$ defined in previous study on cylindrical hollow section columns done by Meng and Gardner [10]. With the column's diameter of $D = 82.5$ mm and the thickness of $t = 3.6$ mm the mesh edge size is of 8.6 mm.

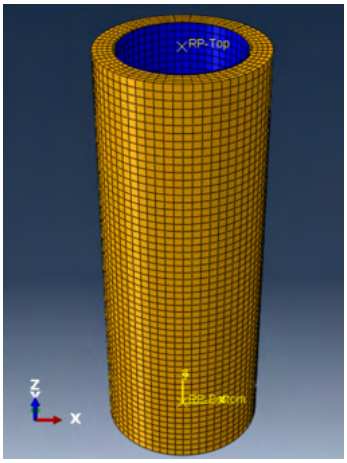

Figure 2.38: Mesh ABAQUS Model S-ST-15

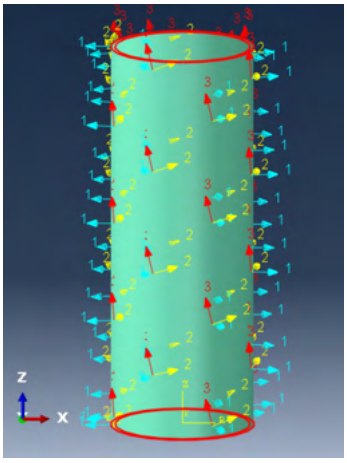

Figure 2.39: Material orientation S-ST-15

In Table 2.4 are summarised the main geometrical parameters for the steel shell for each specimen, namely length L, diameter D_S and thickness t_S. The summary of the dimensions for the timber veneer layer is in Table 2.5 with the mean value of inner ($D_{T,inner}$) and outer diameter ($D_{T,outer}$), partition thickness $t_{T,tot}$ and $t_{T,part}$. A detailed summary of the measurements is visible in Appendix E.

Table 2.4: Dimensions steel shell element

Sample	**L** [mm]	$\mathbf{D}_S$ [mm]	$\mathbf{t}_S$ [mm]
S-S-0	288	78.9	3.6
S-ST-0	280	78.9	3.6
S-ST-15	280	78.9	3.6
L-S-0	2000	78.9	3.6
L-ST-0	2000	78.9	3.6
L-ST-15	2000	78.9	3.6

Table 2.5: Dimensions solid timber element

Sample	**L** [mm]	$\mathbf{D}_{T,inner}$ [mm]	$\mathbf{D}_{T,outer}$ [mm]	$\mathbf{t}_{T,tot}$ [mm]	$\mathbf{t}_{T,part}$ [mm]
S-ST-0	280	82.5	103.1	13.6	3.4
S-ST-15	280	82.5	107.1	15.9	3.975
S-T-0	280	83.7	104.2	10.2	2.55
S-T-15	280	84.1	104.6	10.3	2.575
L-ST-0	2000	82.5	104.6	14.7	3.675
L-ST-15	2000	82.5	105.6	15.1	3.775

The ployurethene glue between the outer steel's surface and the inner timber veneer's layer is modelled with a tie constraint. It is possible to do such assumption because no failure is expected to append in the adhesive layer between the two materials. Two reference points are created in the middle of the cylinder at both ends of the column. They are coupled to the cross section area of the steel and the timber veneer through kinematic coupling as shown in Figure 2.40. At those two reference points are then applied the boundary conditions. At first two hinges are modelled, so the BC constrains all displacement at the bottom and on top lets free the vertical one and allows rotation in all directions. Furthermore, two other layouts are analysed, first the case of a joint at the bottom, meaning that rotation and displacement are fixed in all directions, while the top BC simulate an hinge free to rotate. The second case constraints all directions meaning that there are two joints and the only freedom is the vertical displacement at the top.

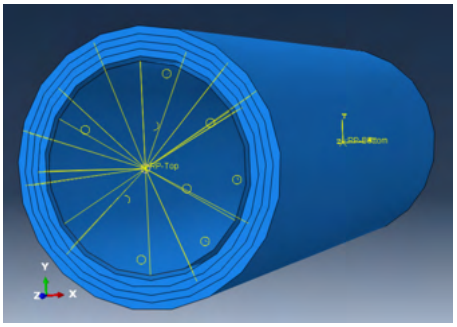

Figure 2.40: View reference point S-ST-15

2.3.2 Material parameters

An important component of the numerical modelling is the i implement the right parameters to simulate the material behaviour. The steel's elastic properties are the Young's Modulus $E = 210GPa$ and the Poisson's ratio $\nu = 0.3$. The plastic behaviour is modelled with a quadri-linear stress-strain relation proposed by Yun and Gardner [11] this engineering stress-strain relation (grey dashed line in Figure 2.41) is then transformed into the true stress-strain relation (black line). Thereby the decrease in the area of the steel profile during the tension test is accounted, which results in the increase of the actual stress in the specimen. The quadri-linear stress-strain relation used is formulated in Equation 2.7. The needed parameters are the Young's Modulus, yield and ultimate strength (defined in the Abnahmeprüfzeugnis of the columns visible in the Appendix A), out of which all other values are derived with the formulas taken from the study of Yun et al. [11] and summarised bellow. The conversion to the true stress-strain relation is done via Equation 2.8. The values of true stress-strain curve, shown in Figure 2.41, are summarised in Appendix F.

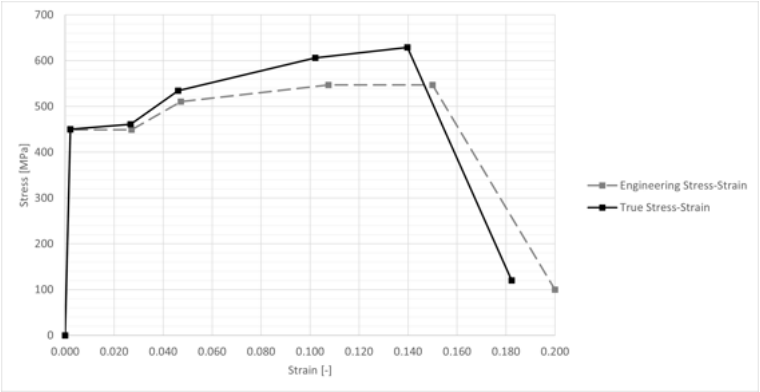

Figure 2.41: Steel Stress-Strain relation

$$f(\varepsilon) = \begin{cases} E \cdot \varepsilon & \text{for } \varepsilon \leq \varepsilon_y \\ f_y & \text{for } \varepsilon_y \leq \varepsilon_{sh} \\ f_y + E_{sh} \cdot (\varepsilon - \varepsilon_{sh}) & \text{for } \varepsilon_{sh} \leq C_1\varepsilon_u \\ f_{C_1\varepsilon_u} + \dfrac{f_u - f_{C_1\varepsilon_u}}{\varepsilon_u - C_1\varepsilon_u} & \text{for } C_1\varepsilon_u \leq \varepsilon_u \end{cases} \tag{2.7}$$

with

$$\varepsilon_u = 0.6(1 - \frac{f_y}{f_u}) \qquad \varepsilon_{sh} = 0.1\frac{f_y}{f_u} - 0.055$$

$$C_1 = \frac{\varepsilon_{sh} + 0.25 \cdot (\varepsilon_u - \varepsilon_{sh})}{\varepsilon_u} \qquad E_{sh} = \frac{f_u - f_y}{0.4 \cdot (\varepsilon_u - \varepsilon_{sh})}$$

$$\begin{cases} \varepsilon_{true} = -\log(1 + \varepsilon_{tot}) \\ \sigma_{true} = \sigma \cdot (1 + \varepsilon_{tot}) \end{cases} \tag{2.8}$$

Contrary to structural steel, the material properties of timber are orthotropic and come with larger uncertainties. The definition of the elastic properties for each direction (R, T, L) is implemented in ABAQUS by means of the feature "Engineering constants". Instead to simulate the plastic behaviour of the veneer the Hill's yield criterion is used. According to recent numerical study done by Akter et al. [12] this criterion has proven to be suitable especially for timber mainly subjected to compression. The shortcoming of this assumption is that the model do not differentiate the response of the material in tension and compression, but since the specimens are loaded in axial compression the tension stresses are assumed to be negligible. The Hill's criterion is defined in ABAQUS by means of the sub-option "Potential", where the input values are the normalised axial and shear strength in the different direction with respect to the axial longitudinal strength.
The calibration of the timber veneer properties is done with the laboratory tests, namely the four point bending test and the tensile test as well as the two compression test on the pure timber sample (S-T-0 and S-T-15). The elastic modules and the axial strength are found from the tests, while the Poisson's ratios, the shear modules as well as the shear strengths are taken from previous studies on similar materials. Moreover the results from the experimental tests are validated by comparing them with indicative values from the literature. The reference elastic values are summarised in Table 2.6. The elastic modules for the radial out-of-plane (E_R) and perpendicular (E_T) direction are assumed to be the same, while the longitudinal modulus (E_L) is higher. The values summarised in Table 2.6 are the tensile stiffnesses taken from the study of Buchelt and Wagenführ [13] who analysed the bending and tensile behaviour of veneer of beech. The values for the shear modules (G_{RT} and G_{RL}=G_{TL}) are taken from the Master thesis of R. Staudacher [14], who tested the bending and shear behaviour of samples made of a dozen of beech veneer glued together. The values for the Poisson's ratio are assumed to be similar to the one for laminated veneer lumbed (LVL), for the two direction radial-perpendicular and perpendicular-longitudinal the reciprocal value are chosen in order to meet the stability condition of ABAQUS and are calculated with Equation 2.9.

$$\nu_{ij} = \frac{\nu_{ji}}{E_j} \cdot E_i \tag{2.9}$$

$\mathbf{E}_R$ [MPa]	$\mathbf{E}_T$ [MPa]	$\mathbf{E}_L$ [MPa]	ν_{RT} [-]	ν_{RL} [-]	ν_{TL} [-]	$\mathbf{G}_{RT}$ [MPa]	$\mathbf{G}_{RL}$ [MPa]	$\mathbf{G}_{TL}$ [MPa]
630	630	12'000	0.20	0.0288	0.0288	100	720	720

Table 2.6: Elastic properties of timber veneer

For the plastic parameters the strength in all direction are needed: in radial and perpendicular direction are assumed to be the same while the one in longitudinal direction is greater, the reference values are taken from the study of Buchlet and Wagenführ [13]. The values reported in Table 2.7 are the tensile strength from the aforementioned research. For the shear strengths as reference are taken the results from the Master Thesis of Staudacher [14]. All values are summarised in Table 2.7 as well as in Appendix G.

$\mathbf{f}_{t,R}$ [MPa]	$\mathbf{f}_{t,T}$ [MPa]	$\mathbf{f}_{t,L}$ [MPa]	$\mathbf{f}_{v,RT}$ [MPa]	$\mathbf{f}_{v,RL}$ [MPa]	$\mathbf{f}_{v,TL}$ [MPa]
7.9	7.9	71.0	11.0	11.0	11.0

Table 2.7: Axial and shear strength of timber veneer

2.3.3 Solving procedure

The ABAQUS model as already said is subjected to a displacement controlled axial compression, meaning that a monolithic increasing displacement is applied to the upper reference point. For the stub columns only a Geometric Material Non-linear Analysis is performed, since global imperfections in sample with low slenderness do not play an important role. The procedure for the long column starts with a Linear-elastic Buckling Analysis (LBA) to find the buckling shapes. The deformation shape of the first mode is then implemented into a Geometric and Material Non-linear Analysis with Imperfection (GMNIA) and amplified with an initial imperfection e_0 according to the draft document prEN 1993-1-14 [15]:

$$e_0[mm] = max\left\{\frac{\alpha \cdot L}{150}, \frac{L}{1000}\right\} \tag{2.10}$$

The imperfection is a function of the buckling length in turn depends on the boundary conditions, therefore three cases are investigated. First both hinges are free to rotate in all directions, the second analysis is done with a top hinge and at the bottom a joint and the third is with two joints, both fixed in all directions. The imperfections are computed with Equation 2.10 with the following values:

- Imperfection factor: $\alpha = 0.21$ according to Tab. 8.2 EN 1993-1-1 [16]
- Buckling length: $L_{Free} = L = 2000\,mm$, $L_{Free-fix} = 0.7 \cdot L = 1400\,mm$ and $L_{Fix} = 0.5 \cdot L = 1000\,mm$

The value of the imperfection are 2.8 mm for the free case, 1.96 mm for the free-fix case and 1.4 mm for the fix case.

Analytical calculation

Moreover, a plausibility check is performed by calculating the plastic resistance of the steel and composite columns according to the Euro Norm 1993-1-1 [16] and comparing it with the maximum peak force from the numerical model. For the composite column the effect of the outer timber veneer layer is accounted by adding the axial strength of the timber to the steel and by using a composite stiffness, which considers the timber Young's Modulus and the increased cross section. The slenderness is therefore changed and computed in the following way:

$$\lambda = \sqrt{\frac{f_y A_S + f_{c,\phi} A_T}{N_{cr} \cdot EI_{comp}}} \tag{2.11}$$

with:

$$EI_{comp} = E_S I_S + E_{T,\phi} I_T \tag{2.12}$$

The final calculation of the plastic resistance take into account the increased area due to the outer veneer layer:

$$N_{pl} = \chi \cdot (f_S A_S + f_{c,\phi} A_T) \tag{2.13}$$

The values used for the cross section area for timber and steel are summarised in Table 2.3. The steel parameters are the following: $E_S = 210$ GPa and $f_S = f_y = 449$ MPa according to Appendix A. The timber values are taken from the compression tests on the timber columns, and both stiffness and strength depends on the angle of inclination of the fibres ϕ.

Chapter 3

Results

In this chapter the results of the three laboratory tests as well as the numerical analysis described in Chapter 2 are presented.

3.1 Four-point bending test

Twenty specimens have been tested with four point bending test, ten for each batch of timber veneer and five for each direction (longitudinal and perpendicular to the fibres). For the longitudinal samples a complete rupture did not occurred as shown in Figure 3.1, instead for the perpendicular one a sudden and brittle failure append for all specimens as visible in Figure 3.2.

Figure 3.1: Sample BS-0-4 after the test

Figure 3.2: Sample BS-90-1 after the test

The parameters measured during the four point bending test are the displacement of the cross head and the force applied. From those values the bending strength of the timber veneer specimens in the two main direction as well as the bending stiffness can be computed respectively with the Equation 2.1 and 2.2. In Figure 3.3 are shown the force-displacement curves for each specimen divided per batch and fibres inclination, for all category the curves are consistent with each other. The longitudinal samples have overall an higher strength compared to the perpendicular ones, while the ductility is similar. In Figure 3.4 is shown the variability of the bending strength over all specimens for each category. Both for the longitudinal and the perpendicular, the strength of the first batch is higher compared to the second. The values are more spread for the longitudinal specimens and reaches higher values. The results of the bending stiffness are summarised in Figure 3.5, as for the strength the specimens with perpendicular fibres are less stiff compared to the longitudinal. Contrary to the bending strength the stiffness reaches higher values for the second batch. In Table 3.1 are summarised the mean value for each batch and each orientation.

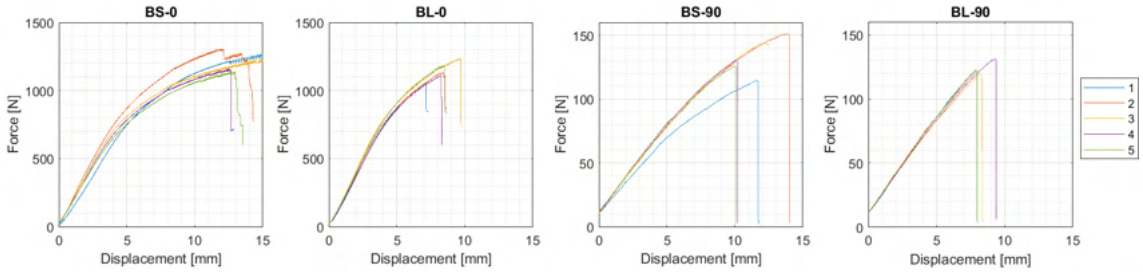

Figure 3.3: Force-Displacement diagram bending test

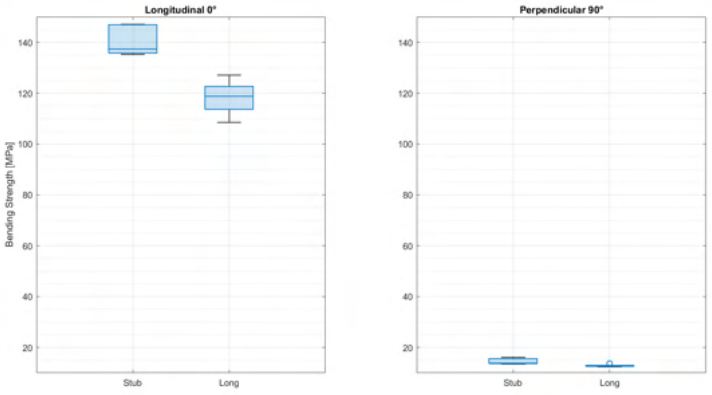

Figure 3.4: Bending strength

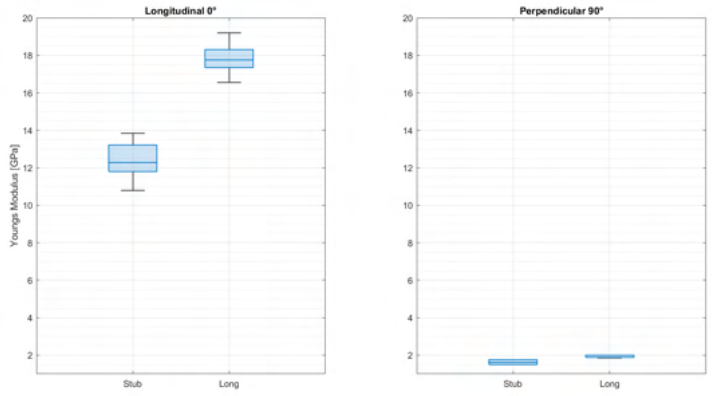

Figure 3.5: Bending stiffness

Sample	**Bending strength** [MPa]	**Bending Stiffness** [GPa]
Stub-0	140.5	12.4
Stub-90	14.5	1.6
Long-0	118.2	17.8
Long-90	12.8	1.9

Table 3.1: Summary bending parameters

3.2 Tensile test

Fourteen specimens for each batch are tested in tension, five of them have the fibres along the loading direction (0), other five have the veneer fibres inclined by 15° and only four are tested with the orientation perpendicular to the main axis. In Figure 3.6 and 3.7 are shown the two failure mode respectively for the diagonal and perpendicular specimens. The longitudinal samples did not reach the failure, because during the loading procedure the grips could not hold the specimen fix and by increasing the tightening force a rupture in the area of the grips occurred. The values of the tensile strength in longitudinal direction are therefore only the lower boundary and not the ultimate strength.

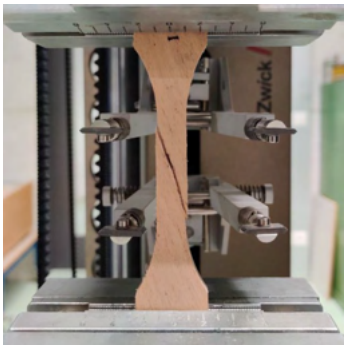

Figure 3.6: Failure of diagonal sample

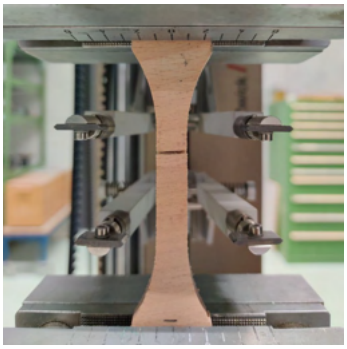

Figure 3.7: Failure of perpendicular sample

The main parameters which define the behaviour in tension are the tensile strength and stiffness, both of them are extrapolated from the stress-strain curves shown in Figure 2.41 using the Equation 2.3 and 2.4. From the following figure can be seen that some specimen had an uncommon behaviour compared to the other one, for this reason sample Nr. 1 for the TS-0 batch, Nr. 2 for the TL-0 and TL-15 as well as Nr. 4 from the TL-90 are not taken into account for the calculation of the strength and stiffness. With the exception of these four cases all other curves are consistent with each other. The tensile strengths are summarised in Figure 3.9, it is visible that the strength decrease with increasing inclination of the veneer fibres. The same can be said for the stiffness as shown in Figure 3.10. The difference between the two batches is way less highlighted compared to the bending behaviour. In Table 3.2 are summarised the mean value of tensile strength and stiffness for the six category. By comparing these values with the one of the literature presented in the previous Chapter there is a minor difference. Those are then used to calibrate the material properties of the timber veneer in ABAQUS.

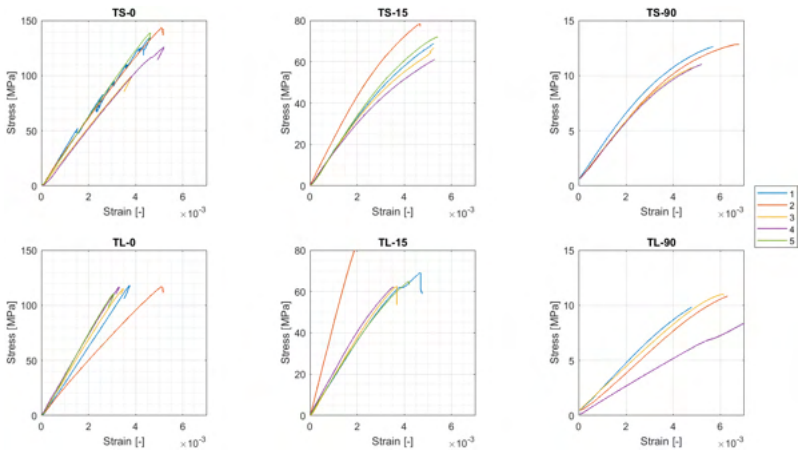

Figure 3.8: Stress-strain tensile test

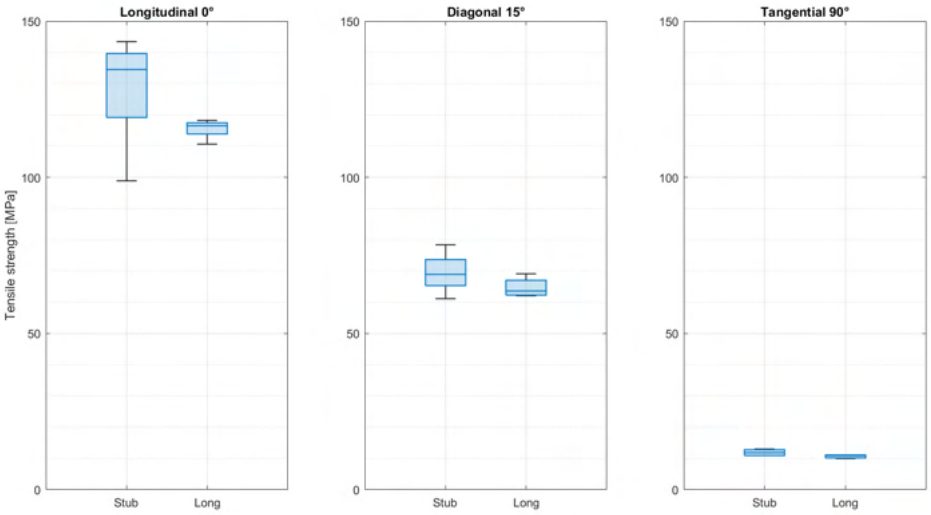

Figure 3.9: Tensile strength

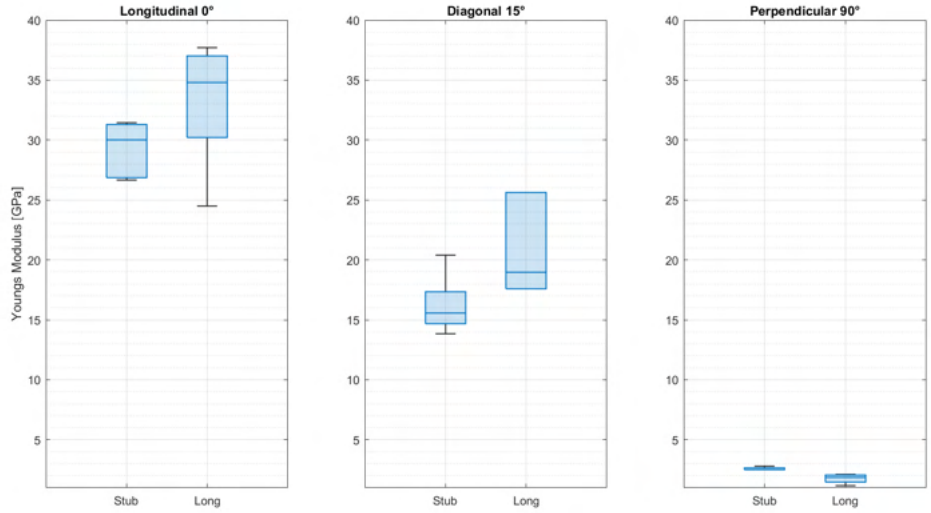

Figure 3.10: Tensile stiffness

Sample	**Tensile strength** [MPa]	**Tensile Stiffness** [GPa]
Stub-0	128.3	29.3
Stub-15	69.5	16.2
Stub-90	11.9	2.6
Long-0	115.5	33.1
Long-15	64.7	18.5
Long-90	10.6	1.9

Table 3.2: Summary tensile parameters

3.3 Axial compression test

The results of the axial compression test on the columns are presented and subdivided per specimen in the form of force-displacement curve, the displacement plotted is the mean values over the measurements of the deformations of the three vertical LVDTs. The main parameters analysed and compared are the stiffness and the maximum force.

Sample S-S-0

The first specimen tested is the pure steel profile, without any timber veneer around also called S-S-0. In Figure 3.11 is shown the force-mean displacement curve superimposed with the measurements of the strain from the DMSs. After an initial elastic phase with a stiffness in the first linear part of 211.9 MPa, when reaching a compression force of around 410 kN and a displacement of 0.5 mm, the plastic phase begins. Right after reaching the yield point, where all DMSs measured a strain of 0.2%, begins the plateau and the loading velocity is increased, this is the cause of the jump visible in the graph. Afterwards is clearly recognisable an hardening phase until reaching the maximum force of 459.9 kN, thereafter a decrease in the force happens and the test is stopped. The ductility of this samples is pretty high since the steel column reached a displacement of almost 9 mm without breaking. Figure 3.12 shows the S-S-0 column after the compression test, it is clearly visible an elephant's foot buckling deformation at the top of the sample. This is a typical instability for cylindrical shell under compression.

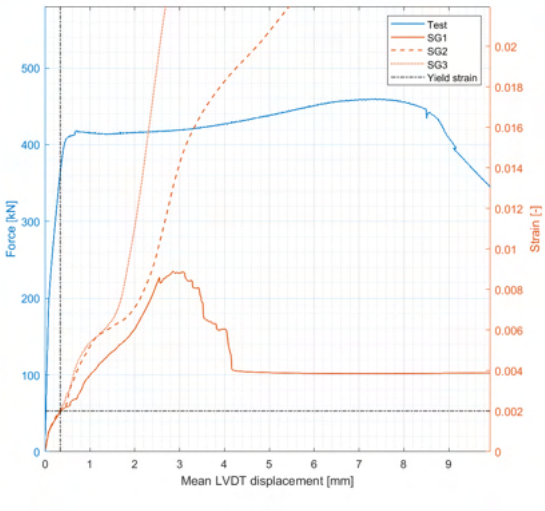

Figure 3.11: S-S-0 Force-Displacement curve

Figure 3.12: S-S-0 after compression

Sample S-ST-0

The first composite stub column tested is the one with the timber veneer fibres orientated along the main axis of the column, also called S-ST-0. Figure 3.13 shows the force-mean displacement curve for the test and the strain measurements. After a initial stiffer behaviour a decrease in the inclination of the curve is visible. The elastic modulus of the composite column, accounting for the increased cross-section area, is of 55.8 MPa. After the initial linear elastic phase, the steel reaches the yielding point where the vertical black dotted line cross the loading curve, this means that after this point the outer timber veneer layer is activated. The yield point of the composite column is reached at a force of almost 555 kN and a displacement of ca. 0.8 mm. The plateau is reached and after short time the maximum force of 575.3 kN is hit which is shortly followed by the decrease in strength and the subsequently drop in structural stability. As for the previous one during the

plastic phase the loading velocity is increased which caused a sudden increase in the force visible in the figure. The column shows some ductility but way lower compared to the pure steel profile, in fact the maximum displacement reached is of ca. 4 mm. Such smaller ductility could be caused by imperfections in the surface where the load is applied. In fact even with small unevenness an eccentricity can cause concentrating overload which results in early failure. In Figure 3.14 is shown the sample S-ST-0 after the test. The upper timber layer is broken and some splits are visible, the inner steel profile buckled in a similar way as the S-S-0 sample. The cracks clearly follow the direction of the fibres, are therefore orientated along the height of the column.

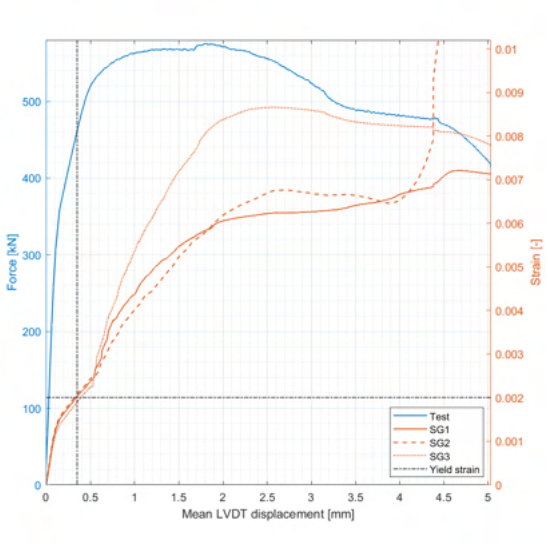

Figure 3.13: S-ST-0 Force-Displacement curve

Figure 3.14: S-ST-0 after compression

Sample S-ST-15

The second composite stub column is built with the timber veneer fibres inclined by 15° with respect to the longitudinal axis, shortened with the name S-ST-15. In Figure 3.15 is shown the force-mean displacement curve of the compression test with the strain measurements from the DMSs. The initial elastic behaviour shows a small decrease in composite stiffness compared to the previous one, the modulus of elasticity reaches a value of 54.0 MPA. When the yield point of the steel profile is surpassed, meaning that all strain gauges have reached the yield strain of steel of 0.2%, the timber is activated at a force of ca. 450 kN. The plastic phase begins after reaching a force of ca. 500 kN and a displacement of 1.2 mm. The plateau shows some jump due to the increase of the loading speed. A maximum force of 521.3 kN is reached and after hitting a displacement of almost 7 mm a decrease in strength arises. The maximum displacement of this composite columns is almost comparable to the one of the bare steel columns, indeed it reached a value of 7 mm. A ductility similar to the steel profile was expected, the small discrepancy could be due to imperfection in the wrapping of the timber veneer or by unevenness at the cross section area. Figure 3.16 shows the S-ST-15 specimen after the compression test. On the bottom part is visible that the timber veneer layers opened up and various cracks following the fibres and spread along the height of the column. This is due to the inner steel profile, which added radial pressure to the timber layer when it starts to buckle. The steel profile inside shows, as before, a typical elephant's foot buckling shape.

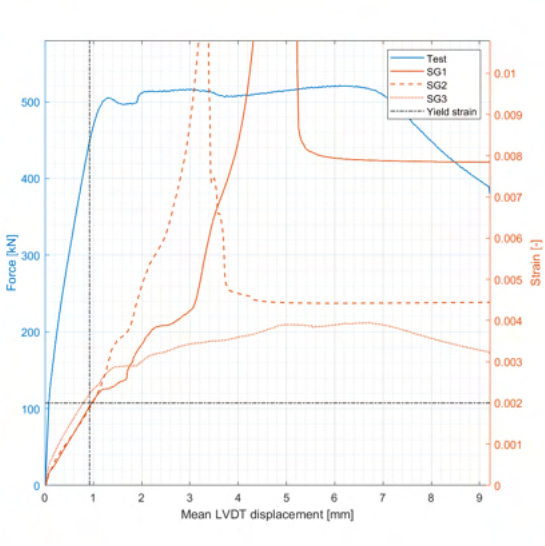

Figure 3.15: S-ST-15 Force-Displacement curve

Figure 3.16: S-ST-15 after compression

Sample S-T-0

After the composite columns the pure timber one are tested. The first has the veneer oriented along the longitudinal direction of the stub column (S-T-0). The Figure 3.17 shows the force-mean displacement curve. A much softer and brittle behaviour compared to the composite and pure steel columns is observed. The elastic phase has an elastic modulus of 12.6 MPa and after reaching the "yield point" at ca. 140 kN is followed by a short plastic phase. The a maximum force of 159.9 kN is shortly reached and then a sudden drop in the strength happens. With the Equation 2.6 is possible to get the axial strength along the longitudinal axis, and results in $f_{c,0} = 57.1$ MPa. The ductility of this sample is way smaller, the maximum displacement reached is of only 2.7 mm. In Figure 3.18 is visible the sample S-T-0 after the test, contrary to the previous specimens almost zero cracks are visible on the outside, but smaller cracks are present inside and mainly situated on the upper part.

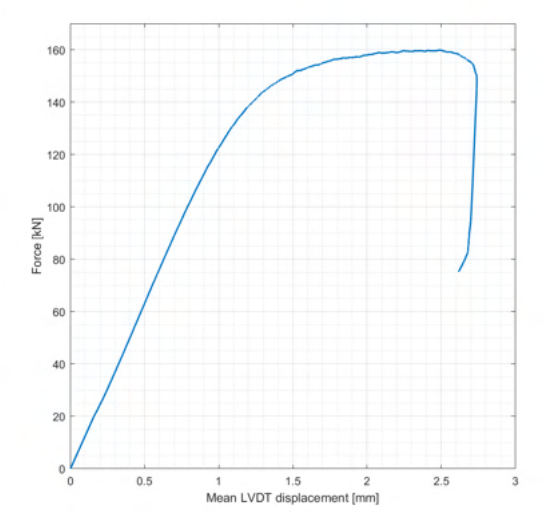

Figure 3.17: S-T-0 Force-Displacement curve

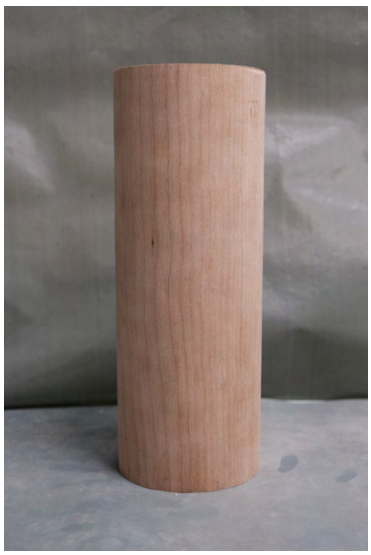

Figure 3.18: S-T-0 after compression

Sample S-T-15

The last stub column tested is the one built with inclined timber veneer fibres and without steel profile inside, also called S-T-15. In Figure 3.19 is shown the force-mean displacement curve. An even brittler behaviour is visible, the plastic phase does not even occur and a sudden loss in strength after an initial phase with inclination of 10.2 MPa is noted after reaching a force of 93.0 kN. From this peak force is possible to compute the compression strength with inclined fibres thanks to the Equation 2.6: $f_{c,15} = 33.4$ MPa. The ductility is even smaller than the previous sample, in fact the maximum displacement which the column could withstand is only of 1.1 mm. The sample S-T-15 after the compression test is shown in Figure 3.20, as the previous timber sample less splits are visible situated this time in the bottom part.

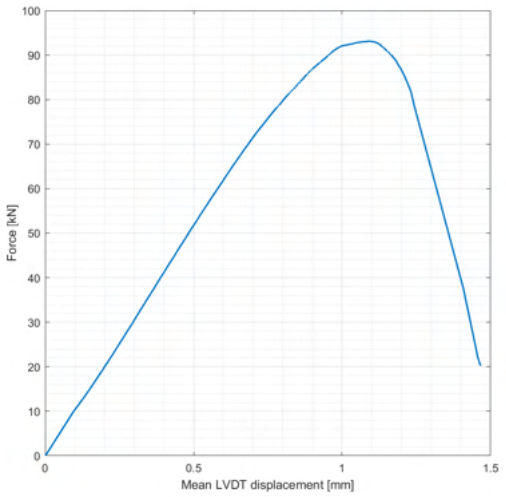

Figure 3.19: S-T-15 Force-Displacement curve

Figure 3.20: S-T-15 after compression

L-S-0

The long steel profile is tested as first, the force-mean displacement curve is visible in Figure 3.21. At the beginning the behaviour seams to be stiffer probably due to the fact that the LVDTs needed some time to settle and start measuring the displacement. Afterwards the elastic linear phase begins with a Young's Modulus of 201.0 MPa, suddenly followed by a instability failure after which the test is stopped. A maximum force of 375 kN is reached at a displacement of ca. 4.4 mm. In Figure 3.22 is shown the deformed column, it is clearly visible that the maximum deformation is situated at an height of ca. 0.7 of the length of the column. This could mean that the hinges did not provided the wanted rotational freedom. The boundary condition are more similar to a fix support.

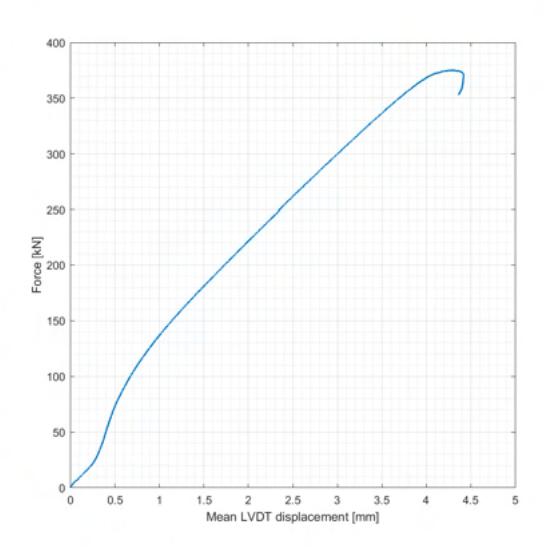

Figure 3.21: L-S-0 Force-Displacement curve

Figure 3.22: L-S-0 after compression

L-ST-0

The first long composite column tested is the one with the veneer aligned to the longitudinal axis of the element. As for the previous one in Figure 3.23 the force-displacement curve shows an initial stiffer behaviour and then the linear elastic phase begins. This time the composite elastic modulus, which account for the increased cross-section area due to the outer veneer layer, is of 54.7 MPa. The maximum resistance is reached at a compression load of 477.8 kN. After reaching the peak an instability failure occurred (global buckling), the force drop and the test is ended. The column after the test is shown deformed in Figure 3.24, the deformed shape is less visible due to the outer timber veneer layer, but as the previous one the boundary conditions seam to be more similar to a fix joint rather than a rotational free one.

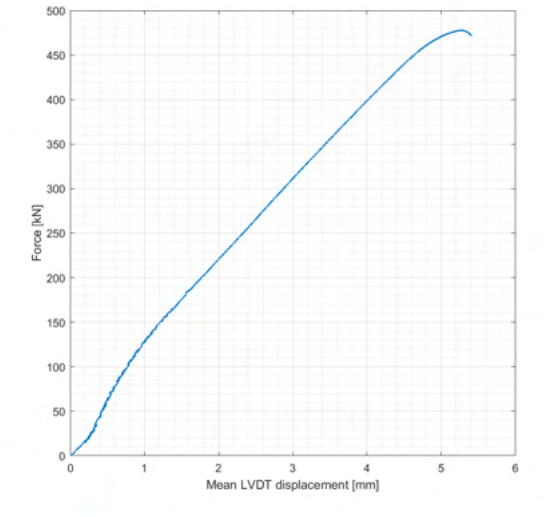

Figure 3.23: L-ST-0 Force-Displacement curve

Figure 3.24: L-ST-0 after compression

L-ST-15

The last column tested is the L-ST-15, with the veneer inclined by 15° with respect to the main axis. In Figure 3.25 is visible the force-mean displacement curve, the same stiffer behaviour can be noted. Moreover, due to technical issues with the vertical LVDTs interfering with the horizontal one, the test was stopped an then continued, this is the cause of the horizontal jump visible in the curve. Thereafter the linear elastic phase with a composite stiffness of 58.0 MPa is followed by the same instability failure after reaching a maximum force of 446.2 kN. The deformed column is visible in Figure 3.26, as before the curve is not highlighted due to the outer timber layer. The bottom part is almost vertical, meaning that the hinge behaves more like a fix joint and blocks the rotation.

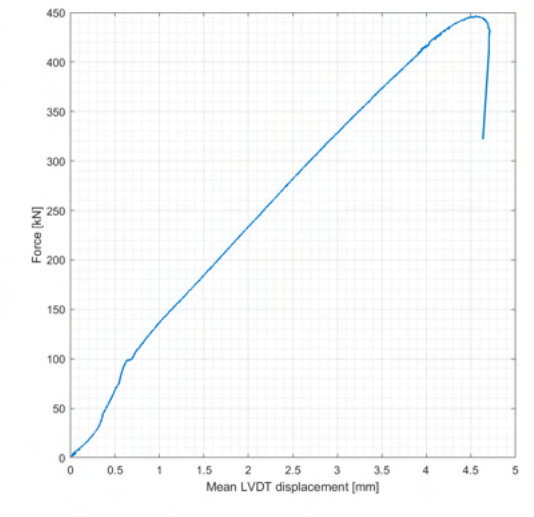

Figure 3.25: L-ST-15 Force-Displacement curve

Figure 3.26: L-ST-15 after compression

3.4 Numerical analysis

As explained in Section 2.3 a numerical model of each column is built. In the following section are presented first the results from the calibration of the veneer material, then the results for stub and long columns.

3.4.1 Timber calibration

The first step before performing the numerical analysis is to calibrate the timber's parameters. The needed value are the longitudinal and perpendicular axial strengths and elastic modules. As presented before in Section 2.3.2 the Poisson's ratios, the shear modules and strengths are taken from previous works. From the material tests the elastic modules as well as axial strengths are computed. All these parameters are highly dependent on the loading direction, from the four-point bending test the values along and perpendicular the fibres are found. The same for the tensile test, which in addition has a third inclination of 15°. Moreover, the axial tests performed on the pure timber columns (sample S-T-0 and S-T-15) serve as additional material test in compression. The dependency of the parameters on the inclination angle is analysed. In Figure 3.27 are shown two subplots, on the left is visible the stiffness normalised with respect to the longitudinal stiffness (E_ϕ/E_0) and on the right the same but for the axial strength (f_ϕ/f_0). In green are shown the results from the tensile test, in red the bending and blue the compression tests. It is highlighted the fact that both stiffness and strength decrease with increasing loading angle.

The perpendicular bending stiffness is 13% the longitudinal one, while for the tensile stiffness the ratio between the two directions is slightly smaller and corresponds to 9%. Since for the compression test only values for inclination 0°and 15°are known, an assumption for the perpendicular value has to be made. The ratio between compression elastic modules $E_{c,90}/E_{c,0}$ is therefore assumed to be equal to the mean value between the ratio for the bending and tensile stiffness, which corresponds to 11%.
The axial strength has a similar trend, for the bending results the ratio between perpendicular and longitudinal value is of 10% and for the tensile of 9%. Also for the axial compression strength only values for an inclination of 0° and 15° are available from the tests. From the analytical formula (13) from SIA 265 [17] the perpendicular axial compression strength is found with the Equation 3.1 reported below with the value for the axial compression strength $f_{c,0} = 57.1$ MPa and $f_{c,15} = 33.4$ MPa found from the timber column tests, the value for the perpendicular direction $f_{c,90} = 1.45$ MPa is extrapolated with $\alpha = 15°$.

$$f_{c,\alpha} = \frac{f_{c,90} \cdot f_{c,0}}{f_{c,0} \cdot sin(\alpha)^2 + f_{c,90} \cdot cos(\alpha)^2} \tag{3.1}$$

From this a first analysis on the behaviour of the compression strength depending on the inclination is done and shown in light blue in Figure 3.27. The loss in compression strength from longitudinal to perpendicular is way higher compared to the bending and tensile one. The ratio $f_{c,90}/f_{c,0} = 2.5\%$ is way smaller compared to the other two tests (ca. 10%). Therefore a second analysis is done by assuming that the ratio between the two main directions is equal to the mean value of bending and tensile results, which corresponds to 10%. In Table 3.3 are summarised the values of elastic modules and axial strengths with 0° and 90° inclinations for the three different tests.

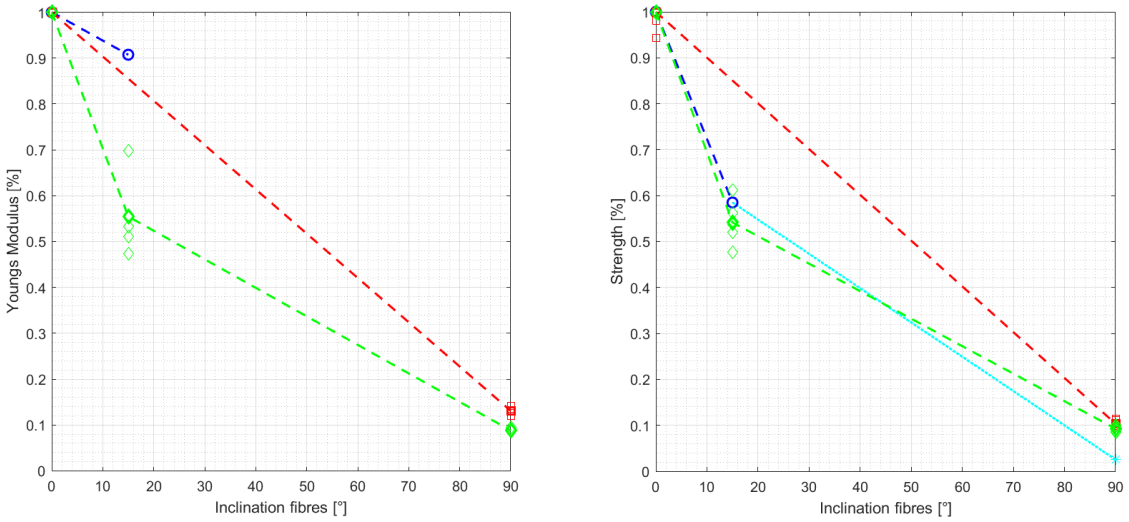

Figure 3.27: Timber parameters analysis

	Tension	**Bending**	**Compression**
E_L [GPa]	29.3	12.4	11.3
$E_T = E_R$ [GPa]	2.6	1.6	*1.23*
$f_0 = f_L$ [MPa]	128.3	140.5	57.1
$f_{90} = f_T = f_R$ [MPa]	11.9	14.5	1.45 (from 3.1) *5.71*

Table 3.3: Elastic modules and strength pro test

To make sure that the parameters are right four simulations are done, one for each test. In Appendix G are summarised the input value for the four simulations. In Figure 3.28 are shown the results, the black curve stands for the compression test which is very similar to the numerical simulation done with the compression stiffness and strength with the assumed ratio of 11% and 10% (blue curve). The second light blue dashed line is the simulation done with $f_{c,90} = 1.45$ MPa from Equation 3.1, the stiffness and maximum strength is identical to the previous one but the behaviour is way more brittle than the experimental test. The red line is the results of the simulation done with the bending strength and stiffness, it is visible that the initial linear elastic behaviour is captured pretty well, the inclination is almost the same as the test but then the ultimate strength is over-predicted. Instead the green curve with the tensile values does not fit at all with the experimental results, this was already clear by looking at the values of tensile strength and stiffness which are both way bigger compared to the compression tests. As conclusion the most suitable parameters to model the behaviour of timber are the one of the dark blue curve, in Table 3.4 and 3.5 are summarised respectively the elastic and plastic input values used in ABAQUS to perform all further simulations.

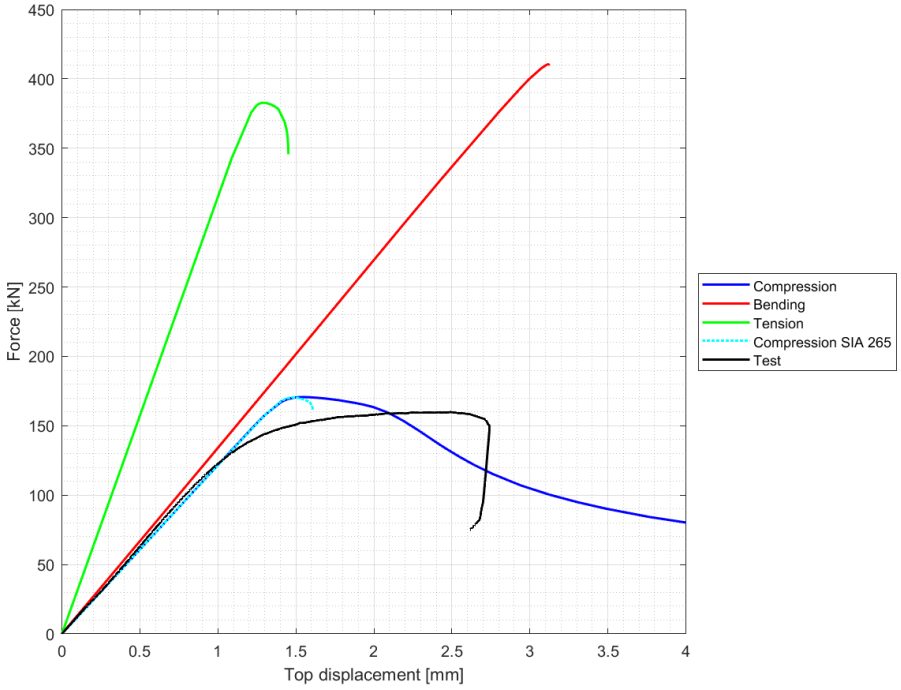

Figure 3.28: Comparison between timber model

$\mathbf{E}_R$ [MPa]	$\mathbf{E}_T$ [MPa]	$\mathbf{E}_L$ [MPa]	ν_{RT} [-]	ν_{RL} [-]	ν_{TL} [-]	$\mathbf{G}_{RT}$ [MPa]	$\mathbf{G}_{RL}$ [MPa]	$\mathbf{G}_{TL}$ [MPa]
1'234.6	1'234.6	11'270	0.20	0.0603	0.0603	100	720	720

Table 3.4: Elastic input values

$\mathbf{f}_y$=$\mathbf{f}_{c,0}$ [MPa]	ε_p [-]	$\mathbf{R}_{11}$ [-]	$\mathbf{R}_{22}$ [-]	$\mathbf{R}_{33}$ [-]	$\mathbf{R}_{12}$ [-]	$\mathbf{R}_{13}$ [-]	$\mathbf{R}_{23}$ [-]
57.1	0	0.10	0.10	1	0.1927	0.1927	0.1927

Table 3.5: Plastic input values

3.4.2 Stub columns

The results form the numerical simulation of the axial compression test on the stub columns are summarised as force-displacement curves in Figure 3.29. The black line corresponds to the pure steel sample S-S-0, the initial elastic phase as a stiffness of 185.3 MPa, after reaching the yield point an hardening effect can be seen. The maximum force reached is of 487.8 kN at a displacement of ca. 16 mm. The ductility is therefore pretty high. The two red lines are the results for the two composite columns S-ST-0 and S-ST-15. The darker one, with fibres inclination 0° reaches the yield point after the steel profile, at a displacement of ca. 2 mm, the plastic plateau is then reached up to maximum force of 663.5 kN. The computed composite stiffness is of 47.7 MPa. For the composite column with 15° inclination (lighter red curve) the behaviour is very similar. The stiffness is a little smaller and reaches a value of 43.1 MPa and on the other hand the maximum force is higher with a value of 673.3 kN. The two smaller curves (yellow and orange) corresponds to the two pure timber specimens, namely S-T-0 and S-T-15. For the former the maximum force is of 170.6 kN and the later only of 136.9 kN. The stiffnesses in the initial linear part are similar and reach respectively the value of 12.2 MPa and 10.4 MPa.

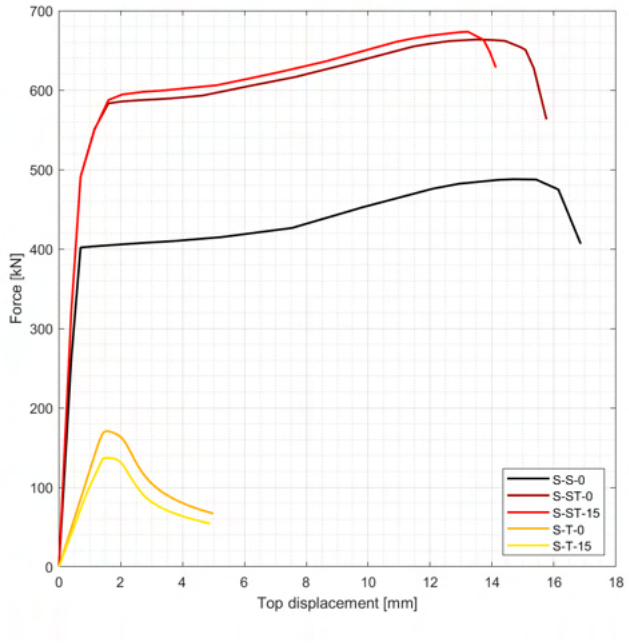

Figure 3.29: Numerical force-displacement curve for stub columns

3.4.3 Long columns

The modelling of the long columns is analogous to the stub one, with the only exception of the boundary conditions. From a first simulation with the same boundary condition as the stub, namely both hinges free to rotate in all directions the results do not match with the experimental results. This is clearly visible in Figure 3.30 where the blue lines for all samples, pure steel L-S-0 as well as for the composite L-ST-0 and L-ST-15, are much lower compared to the test results (black curve). From this first remark a second simulation is performed with a different type of boundary conditions: the bottom hinge constrains the displacement in all direction as well as all rotations. The results (red lines) are more in line with the test but still not exact. Therefore a third analysis is done with both hinges fixed, the outcome are more satisfactory and best represent the experimental results. Hence for all further simulations this layout of boundary conditions is used.

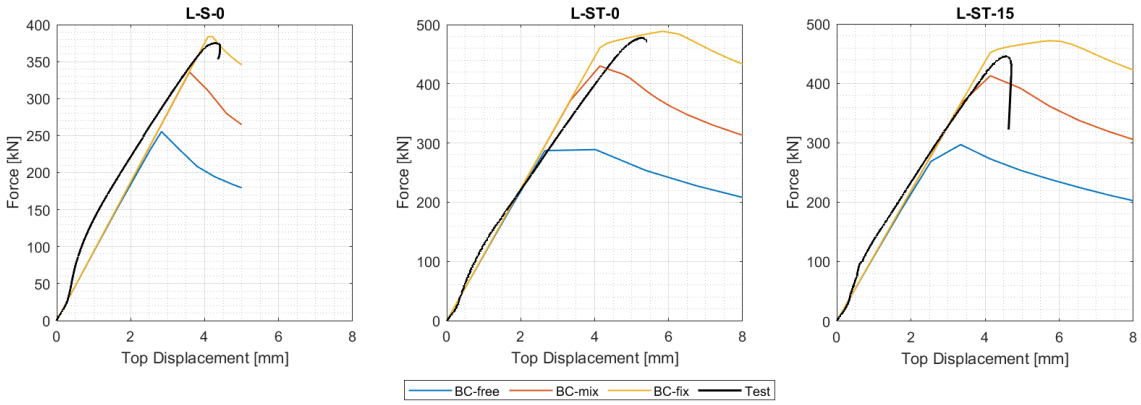

Figure 3.30: Comparison between boundary conditions

In Figure 3.31 are summarised the three final numerical simulation for the long columns. The black curve is the result for the steel profile L-S-0, the first linear elastic phase have a stiffness of 210.2 MPa. After reaching the maximum force of 383.9 kN there is a lost in resistance. For the composite columns both of them reaches higher maximum force 488.8 kN for the L-ST-0 and 472,3 kN for L-ST-15. The inclination in the graph is higher but the actual composite elastic stiffness, accounting the increased CS-area is respectively of 53.7 MPa and 51.0 MPa. The two composite columns show an increased ductility, in fact the peak force is reached at a displacement of ca. 6 mm. After reaching the peak all composite columns seams to still have some resistance, there is not a sudden drop in the force. This is due to the boundary conditions, which are defined as two joints and allow to have a smoother decrease in resistance.
An interesting parameter, which have an important effect on the behaviour of the composite column, is the inclination of the veneer fibres. In Figure 3.31 is shown a fourth force-displacement curve, which is for a column with the veneer inclined by 30°. A trend is clearly visible, by increasing the fibres inclination the benefit in terms of force get progressively smaller.

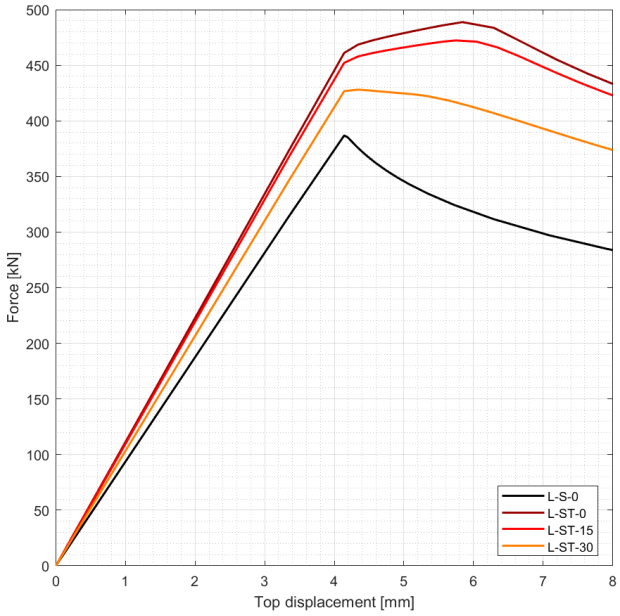

Figure 3.31: Numerical force-displacement curve for long columns

Imperfection influence

The second parameter which influences the behaviour of the columns under compression is the external imperfection. According to the norm [15] as already explained in Section 2.3.3 the imperfection e_0 has a magnitude of 1.4 mm, this is further increased to 2, 4 and 8 mm to see how the resistance changes. In Figure 3.32 are shown four subplots, one for each column layout presented in the previous section, namely pure steel profile (L-S-0) and three composite columns with different fibres inclination (L-ST-0, L-ST-15 and L-ST-30). In each subplot are shown four force-displacement curves for the different imperfection magnitude. It is highlighted that with increasing external imperfection magnitude the maximum force gets smaller and the curve flattens, the initial elastic phase remains unchanged as well as the displacement at which the peak force is reached.

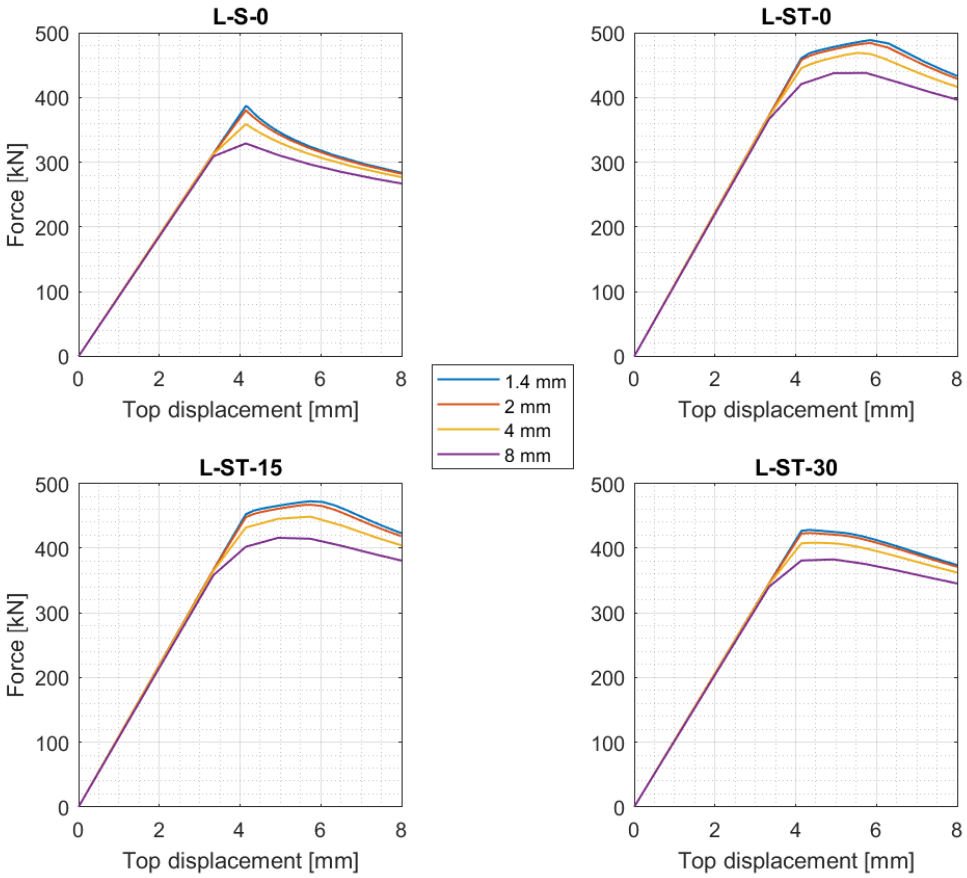

Figure 3.32: Imperfection influence on force-displacement curves

Chapter 4

Discussion

In this chapter the results described in the previous one 3 are discussed. First the comparison between the experimental results of composite and pure steel column is analysed for both stub and long column. Then the relation between experimental, numerical and analytical results is investigated, followed by the detailed analysis of some of the most important parameters, namely the maximum force and the stiffness. Furthermore the influence of the imperfection on the overall behaviour of the columns under axial compression is studied.

4.1 Composite action

In Figure 4.1 are shown two subplots, on the left are reported the experimental results for the stub columns and on the right for the long specimens. On the left graph of Figure 4.1 it is clearly visible that the pure timber specimens (orange and yellow curves) have the lowest strength and ductility, which is a known characteristic of the material timber. Comparing the inclined sample S-T-15 with S-T-0 is evident that the additional rotation of the veneer is disadvantageous in terms of strength and ductility. The perpendicular direction of the veneer is loaded more and since the strength in that direction is way lower compared to the longitudinal ($f_{c,90}/f_{c,0} \cong 10\%$) the ultimate point has a lower value. The pure steel column has an high ductility and strength as expected. With the addition of the outer veneer timber layer around the steel profile there is indeed an increase in the maximum carried force. Both composite stub columns exceed the strength of the S-S-0 sample by 20% and 13% respectively for the S-ST-0 and S-ST-15. This difference in resistance's increase is due, as for the timber columns, to the orientation of the veneer. The ductility on the other hands is decreased by the addition of the outer layer, a similar value is reached for sample S-ST-15 and S-S-0 while S-ST-0 has a decrease of ca. 44%. The cause of such poor results in terms of deformation is the inevitable presence of imperfections due to the manual construction of the composite columns. Unevennesses on the timber surface, where the load is applied, cause eccentricities which lead to concentrated load in some part inducing this early failure.
For the long columns is evident that an instability failure occurred, since either the plateau or hardening effect are present in the force-displacement curves. The only difference between the steel profile and the composite columns is the strength reached, with the specimen L-ST-0 an increase of 27% is achieved while for the L-ST-15 only of 19%. The ductility of the long columns is slightly increased by the addition of the timber veneer with 0° inclination. The maximum displacement for the steel profile is of ca. 4.2 mm, instead for L-ST-0 goes up to 5.2 mm. The sample L-ST-15 reaches similar values as the L-S-0. Overall can be said that the outer timber veneer layer constrains the global buckling of the long columns and delay the instability failure.
By comparing the stub column results with the long ones it is visible that there is a decrease in the strength, this is due to the higher slenderness of the long columns which are more prone to global instability failure.

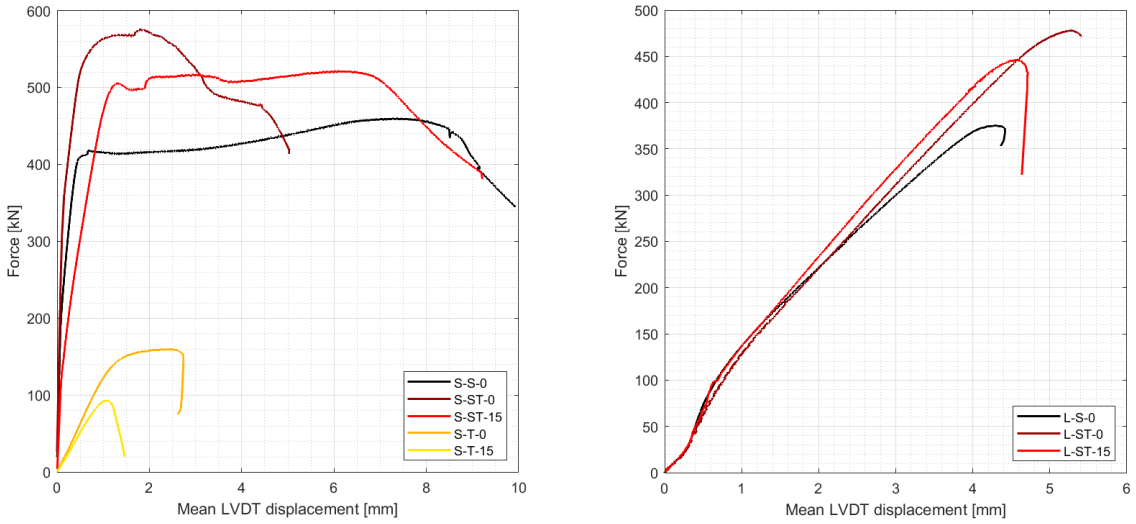

Figure 4.1: Stub/Long- experimental results

4.2 Numerical vs experimental behaviour

In Figure 4.2 and 4.4 are shown three subplots, one for each type of column: pure steel, composite with veneer along the axis and composite with the veneer inclined by 15°. The blue curves represent the experimental test results, whereas the orange dashed lines are the results of the numerical simulations.
For the stub columns the fit between experimental and numerical is not perfect. The short steel profile shows a smaller ductility compared to the ABAQUS results, this could be explained by some imperfections in the profile or by unevenness in the cut surface which are not simulated in the program. The same can be said for the S-ST-0 results, the actual column behaves way more brittle compared to the model. The stiffness and the yielding point is caught pretty well but the specimen suffered of an early failure. The later could result from imperfections in the wrapping procedure or from unevenness in the surface where the load is applied. The last composite stub column (S-ST-15) behaves very differently compared to the numerical results. Yield point, resistance and ductility are over-predicted by the simulation. This is the only case in which the specimen with inclined veneer fibres shows better numerical results compare to the longitudinal one. A possible reason is that the timber material modelling is not that accurate due to the various assumption made to for the inclined veneer. Probably in such small scale (28 cm) the effect of the interpolation between direction has a greater impact on the results compared to the longer specimens.

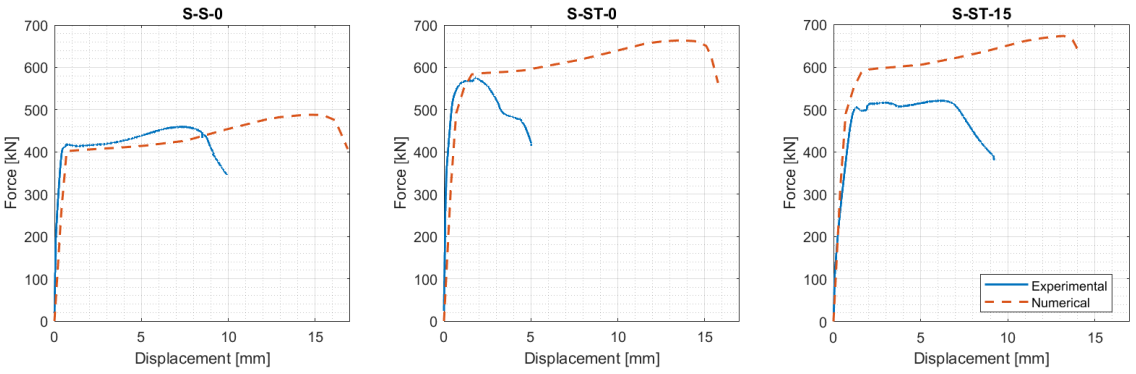

Figure 4.2: Stub column's force-displacement curves

In Figure 4.3 are shown the comparison for the timber columns. On the left for the results for the column without inclination in the veneer. The numerical an experimental results match pretty well, initial stiffness in almost identical, and the maximum force reached is slightly over-predicted by the simulation, while the ductility is slightly smaller. Those good results have to be critically analysed since the results from the test are used to calibrate the properties of the timber material. For the second timber column (S-T-15) on the left the results are not the same, the strength according to the numerical simulation is way higher, as for the previous composite columns, this could be caused by imperfection during the manufacturing process.

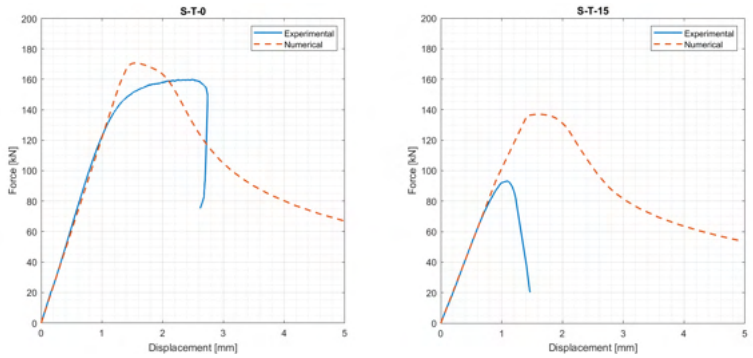

Figure 4.3: Timber column's force-displacement curves

The comparison between numerical an experimental results for the long columns is shown in Figure 4.4. The test outputs are very similar to the ABAQUS one, in all three cases the inclinations of the initial linear elastic phase are well caught as well as the maximum force reached. The only difference is that the numerical simulation have a different behaviour after reaching the maximum force, this is due to the type of constrains implemented in ABAQUS. In the experiment an hinge free to rotate was used as support, at the beginning it behaves as a joint due to the high force applied which increased the frictional resistance at the interface of the spherical part, but once some eccentricity or tilt in the columns happens the hinges start to allow rotation. Therefore, in the test results after reaching the peak force there is a sudden decrease in the resistance due to the instability failure. This is not the case in the numerical model, since both boundary conditions are fixed as joints for the entire test and have a post peak behaviour which still allow to carry some force.

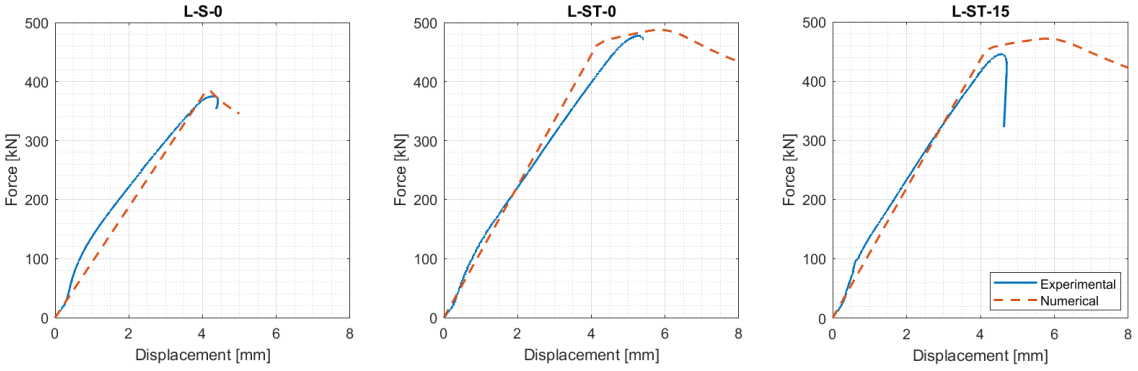

Figure 4.4: Long column's force-displacement curves

4.3 Experimental-Numerical and Analytical parametric investigation

As presented in Section 2.3.3 an analytical plausibility check is performed, this is compared with the experimental and numerical results. The maximum force reached during the axial compression tests is shown in blue in Figure 4.5, the numerical value in orange and in yellow the results from the analytical computations. In Table 4.1 are summarised the vales and the errors with respect to the experimental results.
For the stub columns there is a big difference between test and numerical simulation, as already highlighted in the previous section. The magnitude of the error reaches 29% for the inclined composite column and even 47% for the inclined pure timber specimen. It is not a surprise that the worst results are for the specimens with inclined veneer. The simplistic modelling of the veneer's orientation is a huge assumption, is not clear how the software interpolates the properties of the timber for directions different from the longitudinal, perpendicular and radial one. The result for the timber column with zero inclination has to be critically analysed, because the experimental results were used to calibrate the model, therefore the error is very small. On the other hand the analytical values for the composite columns are more accurate, even better than for the pure steel one. It can be said that the analytical computation for small specimens is reliable and give a good first approximation for the maximum resistance.
The situation is rather different for the long columns, where the numerical results fit better with the experimental than the analytical. The maximum error for the numerical values is of 6% and it is no surprise that it is precisely the one for the inclined sample. Based on this findings, the ABAQUS model is more suitable for longer structure than for shorter one, probably the local effects in modelling the timber material with Hill's criterion and with the inclination defined with a local cylindrical coordinate have a bigger impact in small samples than for longer one.

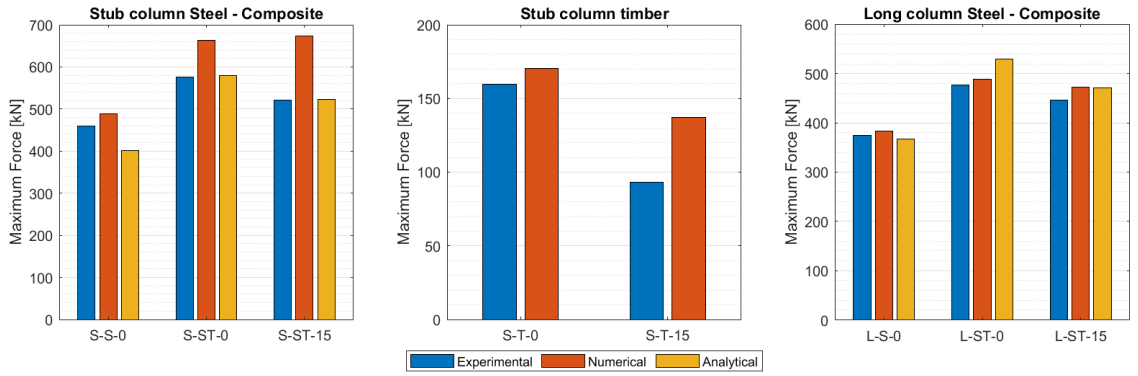

Figure 4.5: Comparison between maximum force

	Experimental	**Numerical**	**Analytical**
S-S-0	459.9	487.8 +**6%**	400.7 **-12%**
S-ST-0	575.3	663.5 +**15%**	579.7 +**1%**
S-ST-15	521.3	673.3 +**29%**	523.0 +**0.3%**
S-T-0	159.9	170.7 +**7%**	-
S-T-15	93.1	136.9 +**47%**	-
L-S-0	375.1	383.9 +**2%**	366.9 +**2%**
L-ST-0	477.8	488.8 +**2%**	530.1 +**10%**
L-ST-15	446.2	472.3 +**6%**	470.7 +**5%**

Table 4.1: Maximum force comparison [kN]

The second parameter compared between numerical and experimental is the stiffness of the column. As shown in Figure 4.6 the overall stiffness of the composite columns, by considering the entire cross section, is smaller compared to the pure steel profile, but bigger than the one for the pure timber column. Between stub and long columns the difference in the stiffness is small, meaning that there is almost zero influence due to the length on the elastic behaviour of the columns. Moreover, can be said that the veneer fibre's inclination do not affect the stiffness. In fact the value for S-ST-0 and S-ST-15 are almost identical, the same can be said for the timber and long columns. In Table 4.2 are summarised the values with the respective errors, the same trend can be seen as for the maximum force, for the stub columns the error is higher compared to the long columns and the prediction of the stiffness for the inclined samples is less precise compared to the longitudinal one.

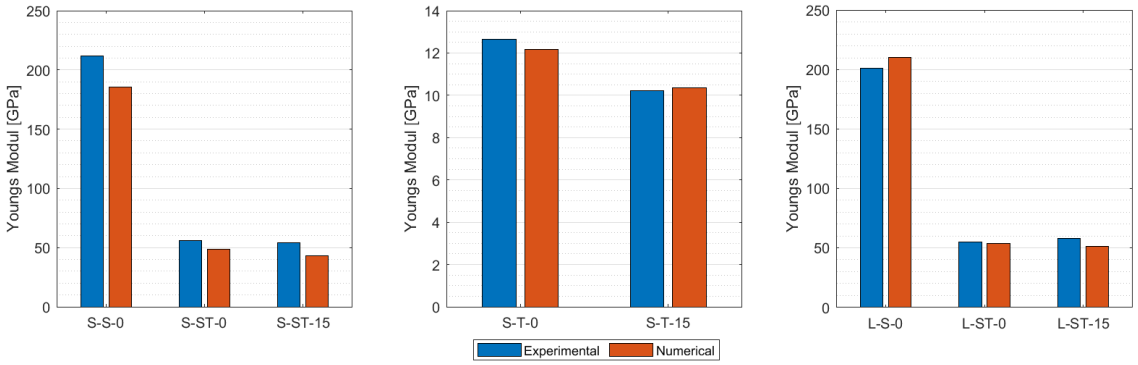

Figure 4.6: Comparison between stiffness

	Experimental	**Numerical**
S-S-0	211.9	185.3 **-12%**
S-ST-0	55.8	48.7 **-13%**
S-ST-15	54.0	43.1 **-20%**
S-T-0	12.6	12.2 **+3%**
S-T-15	10.2	10.4 **+2%**
L-S-0	201.0	210.2 **+5%**
L-ST-0	54.7	53.7 **-2%**
L-ST-15	58.0	51.0 **-12%**

Table 4.2: Stiffness comparison [GPa]

4.4 Imperfection analysis

The results from the simulation with different magnitude of imperfection presented in section 3.4.3 clearly show that there is a decrease in performance by increasing imperfection. This change is further analysed in Figure 4.7 where are shown the percentage force loss for each column with respect to the imperfection defined by the norm. The pure steel profile have the highest drop of 15% in maximum force by an imperfection of 8 mm contrary to the L-ST-0 columns which have a loss of only 10%. The columns with veneer inclined by 30°have a similar behaviour with a loss of ca. 10.5% and the L-ST-15 is situated in between with a drop of almost 12%. The decrease in resistance is not linear and by the steel profile is even more pronounced than for the composite columns. The addition of an external layer of veneer timber decrease the effect of the imperfection on the maximum resistance of the column.

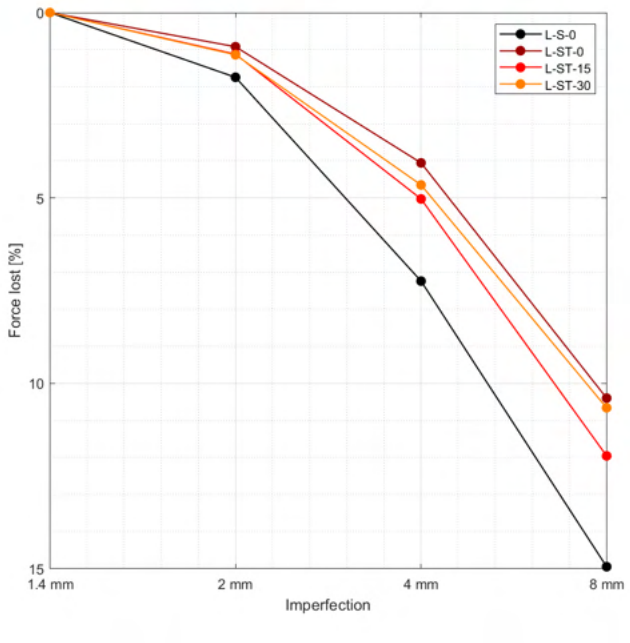

Figure 4.7: Percent force loss due to imperfections

Chapter 5

Conclusion

This master thesis has highlighted the benefit of combining two materials which at first sight do not seam to be compatible. The manual construction of composite steel-timber columns, even if challenging due to the length of the specimens, the inexperience and the relatively poor quality of the timber veneer, is possible and results in samples with small inaccuracy considered all aforementioned impediments.

The steel - timber veneer wrapped columns show an overall increased resistance against axial compression. The composite action helps constraining local and global buckling, thereby delaying the instability and consequently increasing the compression strength. For the short columns an increase of 20% is achieved whereas for the long ones the increment is even higher with a value of 27% as shown in Figure 4.1. With the specimens S-ST-15 and L-ST-15 the effect of the inclination of the veneer fibres on the resistance is analysed and it can be safely concluded that is disadvantageous. This is caused by the orthotropic characteristics of timber, which is also highlighted by the results of the axial compression tests on pure timber columns. The inclination angle's dependency of the axial compression strength is evident from the values of $f_{c,0} = 57.1$ MPa for S-T-0 and $f_{c,15} = 33.4$ MPa for S-T-15. The decrease in resistance due to the increase of inclination of 15° is of 9% for the stub columns and 6% for the long ones.

The numerical study done with the software ABAQUS 3D points out various interesting aspects such as the relevance of material modelling, the huge role of the definition of the boundary conditions as well as the effect of external imperfection on the behaviour of axially compressed columns. The accuracy in modelling the timber veneer behaviour with the Hill's yield criterion, as proposed by Akter et al. [12], combined with the simplistic definition of the veneer fibre's inclination seams to be highly dependent on the size of the specimens. In fact the accuracy in the results for the long columns is way higher compared to the stub ones, the former reaches an error in the range of 2-6% while the later arrives to value of 47%. On the other hand the results for the steel simulation with the quadri-linear stress-strain relation proposed by Yun et al. [11] represent very well the actual behaviour of the steel profile. In fact the error between experimental and numerical results varies between 2 and 6%. Another important factor are the boundary conditions, especially for long structure, where there is a major effect on the overall behaviour. Furthermore, the GMNIA simulations done with different values of imperfection emphasise the benefit in having a composite structure, it reduces the negative effect of imperfections on the resistance as shown in Figure 4.7. As conclusion the modelling of the aforementioned columns with ABAQUS with Hill's yield criterion for timber and quadri-linear stress-strain relation for steel is possible and pretty accurate results are achieved especially for longer samples.

Outlook

Improvement in the numerical simulation could be done by modelling in a more accurate way the hinges with a solid element with the actual geometry and material properties and by considering the effect of friction. In this way the real behaviour of the hinges, which at the beginning act like a joints and after some eccentricity starts to rotate, could be captured and more realistic results could be achieved. Moreover, in terms of timber material modelling a subroutine could be implemented to differentiate between tension and compression, in order to have more accurate results.
In terms of experimental study more columns should be tested, the construction procedure could be improved with automatic vacuum machine and parameters such as the thickness of the timber layer, length and slenderness would be interesting to investigate. Furthermore, the effect of the outer veneer layer on the fire resistance should be analysed.

Appendix A

Abnahmeprüfzeugnis

ŽELEZIARNE PODBREZOVÁ

Inšpekčný certifikát
Inspection certificate
Abnahmeprüfzeugnis
EN 10204:2004/3.1

Číslo
Number
Nummer

60809/1/2022

Č.ext.obj. - External order No. - Externauftragsnummer:
DE220823

Číslo položky - Item number - Positionsnummer:
14

Identifikačné číslo - Ident. number - Ident. numer:
65294

Č.obj.príj. - Consignee order No. - Auftrags Nr.des Empfängers:
4501913894

Číslo zákazky výrobcu - Manufacturer's works order number - Werksauftragsnummer:
SA 255573/1/3 324A379

Číslo dopravného prostriedku - Transport No. - Waggon Nr.:
BJ709CK BJ988YD

Číslo ložného listu - *Loading Bill No.* - *Ladebrief Nr.*:
3024907

Zákazník/Príjemca. - Customer/Consignee - Besteller/Empfänger:

Van Leeuwen Deutschland GmbH & Co.KG
Am Schlütershof 30
47059 Duisburg
GERMANY

Výrobok - *Product* - *Erzeugnis*:

Rúry oceľové bezošvé, valcované za tepla - rúry pre tlakové účely
Seamless hot finished steel tubes - Tubes for pressure purposes
Nahtlose warmgewalzte Stahlrohre - Rohre fur Druckbeanspruchungen

Vonkajší priemer - Outside diameter - Aussendurchmesser:	**82.500** mm	
Hrúbka steny - Wall thickness - Wanddicke:	**3.600** mm	
Dĺžka - Length - Länge:	**6000.000** mm	[-0 +500] mm
Počet kusov - Number of pieces - Stückzahl:	**38**	
Celková dĺžka - Total length - Gesamtlänge:	**230.00** m	
Celková hmotnosť - Total mass - Gesamtmasse:	**1639.00** kg	

Značka výrobcu - *Symbol of the manufacturer's work* - *Herstellerzeichen*

Pečiatka závodného znalca - *Works inspector's stamp* - *Stempel des Werks Sachverstandingen*

Materiál - *Material* - *Material*:

E355+N EN 10297-1 :2003, P355N TC1 EN 10216-3 :2013, S355J2H EN 10210-1 :2006, St 52.0 N DIN 1629 :1984

Stav dodania - *Products as delivered condition* - *Lieferzustand*:

Normalizačné tvárnenie - *Normalizing forming* - *Normalisierendes Umformen*

Technické predpisy - *Technical requirements/Demand* - *Prüfgrundlagen/ Anforderungen*:

AD 2000-Merkblatt W4, VdTUV Werkstoffblatt 354/2, DIN 1629 :1984, EN 10210-1 :2006, EN 10216-3 :2013, EN 10297-1 :2003, EN 10220 :2002, PED 2014/68/EU

Číslo tavby *Cast number* *Schmelze Nr.*	Počet kusov *Number of pieces* *Stückzahl*	Dĺžka *Length* *Länge* [m]	Hmotnosť *Mass* *Masse* [kg]	Druh tavenia *Steelmaking process* *Erschmelzungsart*
25610	**38**	**230**	**1639**	**E**

E = elektrická oblúková pec - *electric arc furnace* - *elektrolichtbogenofen*

Miesto **v Podbrezovej**
Location **ma**
Ort

Dátum **22.11.2022**
Date
Datum

Závodný znalec
Works Inspector
Der Werks Sachverstandige

Ing. Čižmárik Miroslav

ŽELEZIARNE PODBREZOVÁ akciová spoločnosť 976 81 Podbrezová Oddelenie kontroly a zabezpečovania kvality -1-

ŽELEZIARNE PODBREZOVÁ

Inšpekčný certifikát
Inspection certificate
Abnahmeprüfzeugnis
EN 10204:2004/3.1

Číslo
Number
Nummer

60809/1/2022

Druh ocele - *Steel grade* - *Stahlsorte*:

úplne ukľudnená oceľ - *fully killed steel* - *vollberuhigter Stahl*

Úprava povrchu - *Surface protection* - *Oberflächenschutz*:

Bez úpravy povrchu (neolejované) - *Without surface treatment (without oil)* - *Ohne Oberflächenbehandlung (ungeölt)*

Chemické zloženie - *Chemical composition* - *Chemische Zusammensetzung*:

Číslo tavby *Cast number* *Schmelze Nr.*		C [%]	Mn [%]	Si [%]	P [%]	S [%]	Cu [%]	Cr [%]	Ni [%]	Al [%]	Mo [%]	Ti [%]	V [%]	Nb [%]
	Predpis - *Requirements* - *Vorschrift*													
	min.		0.90							0.020				
	max.	0.20	1.60	0.50	0.025	0.020	0.30	0.30	0.50		0.08	0.040	0.100	0.050
25610		**0.17**	**1.23**	**0.20**	**0.017**	**0.007**	**0.23**	**0.07**	**0.07**	**0.029**	**0.02**	**0.001**	**0.002**	**0.000**

Číslo tavby *Cast number* *Schmelze Nr.*		N [%]
	min.	
	max.	0.0200
25610		**0.0080**

Skúška ťahom - *Tensile test* - *Zugversuch* : **20** °C

	Číslo tavby *Cast number* *Schmelze Nr.*	Vzorka č. *Test sample No.* *Probe Nr.*	Rozmery *Dimensions* *Masse* [mm]	Smer odberu/typ vzorky *Direction/Type of the test piece* *Probenrichtung/ Probenform*	Medza klzu *Yield point - Proof stress* *Streck - Dehngrenze* ReH [MPa]	Pevnosť v ťahu *Tensile strength* *Zugfestigkeit* Rm [MPa]	Ťažnosť *Elongation* *Bruchdehnung* A5,65 [%]
C. Nr	Predpis - Requirements - Vorschrift:				min.	355	500	22.0
					max.	---	630	---
1	**25610**	A057443/22	12.64x3.60	L / V		**449**	**547**	**29.7**

L = Pozdĺžny - *Longitudinal* - *Längsrichtung*

V = Výrez - *Strip test* - *Streifen*

Skúška stlačením vyhovela.
Flattening test without objections.
Faltversuch ohne Beanstandung.

Skúška rozširovaním prstenca vyhovela.
Ring expanding test without objections.
Ringaufdornversuch ohne Beanstandung.

Skúška rozširovaním vyhovela.
Flaring test without objections.
Aufweitversuch ohne Beanstandung.

Systém kvality výrobcu je certifikovaný fy SGS podľa ISO 9001, číslo certifikátu HU95/4628, platnosť certifikátu je do 15.6.2023.
Producer´s Quality Assurance Sytem is certified according to ISO 9001 by SGS, certificate no. HU95/4628, validity: 15.6.2023.
Das Qualitätssystem des Herstellers ist nach ISO 9001 von SGS zertifiziert, Zertifikatsnummer HU95/4628, Gültigkeit bis 15.6.2023.

Miesto **v Podbrezovej**
Location
Ort
ma

Dátum **22.11.2022**
Date
Datum

Závodný znalec
Works Inspector
Der Werks Sachverstandige

Ing. Čižmárik Miroslav

Železiarne Podbrezová a.s., Kolkáreň 35, 976 81 Podbrezová, Slovak Republic
Phone: +421 48 645 3031, Fax: +421 48 645 3032, www.steeltube.sk
CIN: 31 562 141, VAT No: SK2020458704
Bank account: Slovenská sporiteľňa, a.s., IBAN: SK69 0900 0000 0000 7990 0086, SWIFT (BIC): GIBASKBX
Registered in Register of Business Names in the District Court Banská Bystrica, Section Sa, Entry No. 69/S

ŽELEZIARNE PODBREZOVÁ akciová spoločnosť 976 81 Podbrezová Oddelenie kontroly a zabezpečovania kvality -1-

Rádioizotopická aktivita je max. 100 Bq/kg.
Radioisotopic activity is max. 100 Bq/kg.
Radioisotopische Aktivität ist max. 100 Bq/kg.

Skúška vírivými prúdmi vyhovela EN ISO 10893-1. 100%.
Eddy current test without objections EN ISO 10893-1. 100%. .
Wirbelstromprüfung ohne Beanstandung EN ISO 10893-1. 100%.

Skúšky ťahom za tepla podľa AD 2000-Merkblatt W4, časť 3.3 neboli vykonané so súhlasom TÜV NORD Systems, TÜV-file:18B03/012.
With the approval of TÜV NORD Systems,TÜV-file:18B03/012, hot tensile tests according to AD 2000-Merkblatt W4, section 3.3 have not been carried out.
Verzicht auf Warmzugversuche gemäss AD 2000-Merkblatt W4, Abschnitt 3.3 mit Zustimmung der TÜV NORD Systems, TÜV-Az.:18B03/012.

Inšpekčný certifikát EN 10204 3.1 podľa AD 2000 W4 , časť 5.1, vydaný na základe písomného súhlasu TÜV NORD Systém, TÜV–dokument 1326W133360.
Inspection certificate EN 10204-3.1 acc. to AD 2000-Guideline W4, sec. 5.1; letter of agreement by TÜV NORD Systems; TÜV-file 1326W133360.
Abnahmeprüfzeugnis EN 10204-3.1 gemäß AD 2000-Merkblatt W4; Abs. 5.1; Zustimmungsschreiben der TÜV NORD Systems. TÜV-Az.: 1326W133360.

Systém kvality výrobcu bol podrobený špecifickému hodnoteniu pre materiály (Článok 4.3 a 7.5, Príloha I Smernice PED 2014/68/EU). Certifikát 07/202/9150/WZ/0915/20 vydalo notifikované miesto 0045 TÜV NORD Systems GmbH s platnosťou do 02/2023. Rozsah platnosti certifikátu zahŕňa predmetné výrobky.
The producer has a specific reviewed quality system for materials according to the Article 4.3 and 7.5, Annex I of the Directive PED 2014/68/EU. The certificate 07/202/9150/WZ/0915/20 with the validity till 02/2023 was issued by the Notified Body TÜV NORD Systems GmbH, Code 0045. The mentioned products belong to the certificate validity range.
Der Hersteller hat ein spezifisch beurteiltes Qualitätssystem für die Werkstoffe nach dem Artikel 4.3 und 7.5, Anhang I der Direktive DGRL 2014/68/EU. Das Zertifikat 07/202/9150/WZ/0915/20, gültig bis 02/2023, wurde von der Benannten Stelle TÜV NORD Systems GmbH, Kennummer 0045 erstellt. Die aufgeführten Produkte sind im Geltungsbereich des Zertifikates eingeschlossen.

Všetky výrobky vyhovujú vyššie uvedeným normám a požiadavkám v objednávke.
All products meet requirements of above mentioned standards and requirements specified in the order.
Alle Produkte entsprechen den o.a. Normen und Forderungen in der Bestellung.

Vizuálna kontrola a rozmery vyhoveli (100 %).
Visual inspection and dimensional check without objections (100 %).
Visuelle Kontrolle und Abmessungskontrolle sind in Ordnung (100 %).

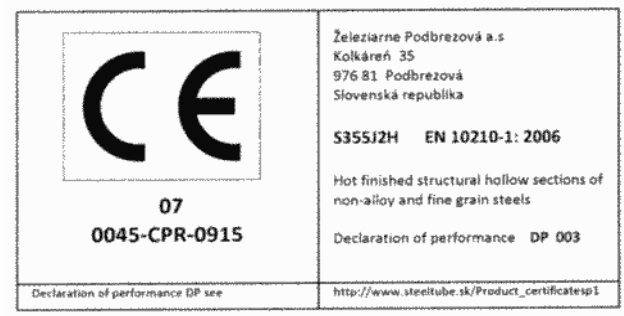

Overenie základných parametrov dokumentu kontroly v informačnom systéme výrobcu ŽP a. s.:
Verification of basic parameters of inspection document in the ZP information system (Manufacturers information system):
Die Verizifierung der Grundparameters der Prüfbescheinigung im ZP Informationssystem (Herstellers Informationssystem):
https://check.zelpo.sk/certchk.php?ID=170096033

Miesto **v Podbrezovej**
Location **ma**
Ort

Dátum **22.11.2022**
Date
Datum

Závodný znalec **Ing. Čižmárik Miroslav**
Works Inspector
Der Werks Sachverstandige

ŽELEZIARNE PODBREZOVÁ akciová spoločnosť 976 81 Podbrezová Oddelenie kontroly a zabezpečovania kvality -1-

Appendix B

Technical data sheet glue

LOCTITE® HB S309 PURBOND

1K-PUR Klebstoff zur Herstellung von tragenden Holzbauteilen
Offene Zeit 30 Minuten

Anwendungsbereich

Der 1K-Polyurethanklebstoff härtet unter Einfluss von Material- und Luftfeuchte zu einem harten, unsprö-den Film aus. Die LOCTITE HB S-Klebstoffe wurden für die Herstellung von Brettschichtholz und Keilzinken-verklebung entwickelt und geprüft. Weitere Anwen-dungen sind Verbindungen von Holz und Holzwerk-stoffen im nichttragenden Bereich. Für tragende passgenaue Holzverbindungen im Elementbau - Rip-penplatten oder Hohlkastenträger - beinhaltet dieses Merkblatt spezielle Verarbeitungsbedingungen, wel-che einzuhalten sind.

Spezielle Eigenschaften:
LOCTITE HB S Klebstoffe sind als Typ I Klebstoff klassi-fiziert und gemäss Seite 2 dieses Merkblattes (siehe Zulassungen) zugelassen und registriert.
LOCTITE HB S Klebstoffe sind ohne Zusatz von Lö-sungsmittel und Formaldehyd hergestellt und erfül-len die Anforderungen gesunder und ökologischer Bauweise von MINERGIE-ECO®

Produktdaten

Basis:
Isocyanatprepolymer
Viskosität:
Ca. 24'000 mPa.s (Brookfield 20 °C / 20 rpm)
Spezifisches Gewicht:
Ca. 1,16 g/cm^3
Farbe:
Beige
Festkörpergehalt:
100 % und frei von Fasern und abrasiven Füllstoffen
Feuergefährlichkeit:
Schwer entflammbar
Beständigkeit:
Gegen schwache Alkalien, Säuren und Lösungsmittel

Produktdaten (Fortsetzung)

Gebinde / Art-Nr.:
20 x 600 ml Schlauchbeutel / 1519.9533.04
50 kg Fass / 1519.9533.09
200 kg Fass / 1519.9533.11
Zubehör Schlauchbeutel / Art-Nr.:
Handauftragspistole / 8110.9905.01
Druckluftauftragspistole / 8110.9907.01
Mehrlochdüse mit Adapter / 8110.9906.09
Adapter zu Düsen / 8110.9906.01
Dreiecksdüse / 8110.9906.02
Spitzdüse / 8110.9906.03
Trennspray Acmos 100-2450, 400 ml / 2776.9810.27
Reiniger 9797, 500 ml Flasche / 2423.9797.01
Reiniger 9797, 3,79 kg Kanister (5 l) / 2423.9797.02
Zubehör Fass / Art-Nr.:
LOCTITE Trennpaste, 1kg Metalldose / 2770.9817.01
LOCTITE Trennmittel, 800 g Flasche / 2778.9816.01
LOCTITE Trennmittel, 10 kg Kanne / 2778.9816.03
LOCTITE Löser, 3kg Kanne / 2419.9815.02
LOCTITE Sperrmittel, 1 kg Dose / 2055.9814.01
LOCTITE Sperrmittel, 10 kg Kanister / 2055.9814.03

Beachten Sie bitte die Technischen Merkblätter des Zubehörs.

Verarbeitungsdaten

Verarbeitungstemperatur:
(für Umgebung, Material und Klebstoff)
Tragende Anwendung: +15 °C bis +30 °C
Nicht tragende Anwendung: +10 °C bis +35 °C
Bei einer Verarbeitung bei 10 °C verlängert sich die Presszeit um mindestens +50 %. Bei einer Verarbei-tung bei 30 °C verkürzt sich die offene Zeit um ca. mi-nus 30 %
Vorbehandlung Klebeflächen:
Die zu verklebenden Flächen müssen passgenau, sau-ber, staubfrei und fettfrei sein. Lärche ist im Voraus mit Primer PR152 zu behandeln.
Holzfeuchtigkeit:
Tragende Anwendung: 8 % bis 15 %. Die Feuchtedif-ferenz der zu verklebenden Teile darf höchstens 4 % betragen.
Nicht tragende Anwendung: 8 % bis 18 %

LOCTITE® HB S309 PURBOND

Verarbeitungsdaten (Fortsetzung)

Auftragssystem:
Schlauchpresspistole mit Düse, Spachtel, Düsenauftragsgeräte oder andere geeignete Applikatoren. 1K-PUR-Klebstoffe reagieren mit Feuchtigkeit. Bei Fässern ist die Zuluft mit einem feuchtigkeitsabsorbierenden Filter zu trocknen. Maschinenteile, die mit Klebstoff in Berührung kommen, sollten vorgängig mit Trennmittel behandelt werden.

Klebstoffauftrag:
Der Klebstoff wird einseitig aufgetragen. Die aufgetragene Klebstoffmenge muss eine gleichmässige und vollständige Benetzung der Fügeteiloberfläche gewährleisten. Am Rand der Klebefuge muss durchgehend Klebstoff austreten.

Auftragsmenge:
150 g/m^2 bis 200 g/m^2

Offene Zeit (OZ):
30 Minuten (bei 20 °C / 65 % r.F.).
Sofort, aber spätestens 30 Minuten nach Beginn des Klebstoffauftrages (maximale Wartezeit) müssen die zu verklebenden Teile zusammengefügt und der Pressdruck aufgebracht sein. Die maximale Wartezeit der feuchtigkeitsreaktiven LOCTITE HB S Klebstoffe werden von der Luft- und Materialfeuchte sowie von den Umgebungstemperaturen beeinflusst. Höhere Temperaturen und höhere Luftfeuchte verkürzen die Wartezeit. Das Aufbringen des Pressdruckes muss zwingend vor einer allfälligen Hautbildung auf der Klebstoffoberfläche erfolgen.

Pressdruck:
Tragende Anwendung: 0.6 bis 1 N/mm^2 (6 bis 10 kg/cm^2). Der aufgebrachte Pressdruck muss eine passgenaue Fuge gewährleisten.
Nicht tragende Anwendung: mindestens 0.3 N/mm^2

Presszeit:
75 Minuten (20 °C / 65 % r.F.).
Die Presszeit ist abhängig von Temperatur und Feuchtegehalt der Fügeteile und der Umgebung. Tiefere Temperaturen und Luftfeuchte verzögern den Abbindeprozess, höhere Temperaturen und Luftfeuchte beschleunigen den Abbindeprozess. Die Mindestpresszeit für gerade Träger bei 20 °C, 65 % relativer Luftfeuchte und einer Holzfeuchte von 12% beträgt 75 Minuten, sofern eine optimale Passung der Fügeteile (Fugendicke ≤0,1 mm) gewährleistet ist. Ist eine passgenaue Fuge nicht gewährleistet (maximal 0.3 mm), muss die Presszeit mindestens 90 Minuten betragen. Während der Aushärtezeit (Presszeit) des Klebstoffes dürfen die Klebefugen nicht belastet werden.

Verarbeitungsdaten (Fortsetzung)

Nachlagerzeit:
Nach Ablauf der Presszeit sind die verklebten Bauteile während mindestens 4 Stunden bei 20° C zu lagern. Die Teile können während der Nachlagerzeit bearbeitet werden, wobei die Klebstofffugen jedoch nicht belastet werden dürfen.

Reinigung:
Auftragsgeräte vor der Aushärtung des Klebstoffes mit Reiniger 9797.

Sicherheitshinweis:
Bei harten Laubhölzern und harten Exoten ist eine Probeklebung unerlässlich.

Eigenschaften der Klebstoff-Fuge

Wärmebeständigkeit:
EN 14292: >+150 °C

Wasserbeständigkeit:
EN 204-D4

Bindefestigkeit:
EN 204-D1

Zulassungen

Allgemeine bauaufsichtliche Zulassung vom DIBt (Deutsches Institut für Bautechnik) für die Herstellung von tragenden Holzbauteilen.
Zulassungsnummern: **Z-9.1-765**
Bestätigung von der MPA Universität Stuttgart zur Übereinstimmung mit EN 14080. Der Klebstoff kann für die Herstellung von Brettschichtholz nach EN 14080 verwendet werden.
Geprüft nach EN 15425 und klassifiziert als Typ I Klebstoff zur Verwendung in allen Nutzungsklassen.

Bei tragenden Anwendungen sind die jeweilig gültigen länderspezifischen Produktenormen zu beachten. Zur Gewährleistung einer hohen Verklebungsgüte wird eine geeignete Eigenüberwachung empfohlen.

LOCTITE® HB S309 PURBOND

Sicherheit und Umwelt

Schutzmassnahmen:
Alle Informationen entnehmen Sie der Etikette auf dem Gebinde oder dem Sicherheitsdatenblatt.
Entsorgung Gebinde:
Kontaminierte Verpackungen sind optimal zu entleeren. Gebinde mit ausgehärteten Klebstoffrückständen können auf dem üblichen Weg entsorgt werden (Hausmüll, Altmetall).
Entsorgung Klebstoff:
Nicht ausgehärtete Klebstoffreste können unter Beachtung der örtlichen Amtsvorschriften als Sondermüll entsorgt werden. Nicht in die Kanalisation gelangen lassen.
Abfallcode:
08 04 09 - Klebstoffe- und Dichtmassenabfälle, die organischen Lösemittel oder andere gefährliche Stoffe enthalten.

Lagerung

In dicht verschlossenen Originalgebinden bei +15 bis +25 °C trocken lagern. Vor Frost schützen. Vor Gebrauch umrühren. Beachten Sie das auf dem Gebinde aufgedruckte Verbrauchsdatum.

Auskunftgebende Stelle

Für anwendungstechnische Fragen steht Ihnen unser Beratungsdienst gerne zur Verfügung.

Erstelldatum

26.09.2016 - ersetzt alle früheren Ausgaben

Appendix C

Geometry four point bending specimens

Geometry four point bending specimens

12.06.2023

Dimension in mm

First batch: Stub columns

	BS-0					BS-90				
	1	2	3	4	5	1	2	3	4	5
Thickness	8.55	8.66	8.52	8.61	8.65	8.40	8.59	8.63	8.40	8.74
	8.65	8.65	8.60	8.61	8.64	8.50	8.52	8.57	8.53	8.59
	8.60	8.56	8.64	8.58	8.61	8.65	8.53	8.54	8.56	8.71
Mean Thickness	**8.60**	**8.62**	**8.59**	**8.60**	**8.63**	**8.52**	**8.55**	**8.58**	**8.50**	**8.68**
Standard deviation	**0.05**	**0.06**	**0.06**	**0.02**	**0.02**	**0.13**	**0.04**	**0.05**	**0.09**	**0.08**
Width	18.74	21.48	19.35	18.09	18.15	19.30	21.34	20.50	20.36	19.26
	18.74	21.33	19.29	18.25	18.38	19.25	20.85	20.91	21.68	19.62
	19.24	20.22	19.14	19.13	18.15	19.20	21.01	20.52	22.38	20.47
Mean Width	**18.91**	**21.01**	**19.26**	**18.49**	**18.23**	**19.25**	**21.07**	**20.64**	**21.47**	**19.78**
Standard deviation	**0.29**	**0.69**	**0.11**	**0.56**	**0.13**	**0.05**	**0.25**	**0.23**	**1.03**	**0.62**

Second batch: Long columns

	BL-0					BL-90				
	1	2	3	4	5	1	2	3	4	5
Thickness	8.6	8.75	8.79	8.68	8.66	8.72	8.83	8.88	8.76	8.81
	8.69	8.79	8.9	8.8	8.8	8.74	8.8	8.75	8.73	8.78
	8.65	8.72	8.75	8.75	8.67	9.1	8.81	8.6	8.77	8.81
Mean Thickness	**8.65**	**8.75**	**8.81**	**8.74**	**8.71**	**8.85**	**8.81**	**8.74**	**8.75**	**8.80**
Standard deviation	**0.05**	**0.04**	**0.08**	**0.06**	**0.08**	**0.21**	**0.02**	**0.14**	**0.02**	**0.02**
Width	21.28	19.91	20.6	20.45	20.89	20.56	20.4	20.66	21.12	21.12
	21.2	20.33	20.28	20.58	20.94	20.61	20.31	20.25	20.7	20.7
	20.87	20.3	20.04	20.26	20.85	20.05	20.22	21.08	20.04	20.04
Mean Width	**21.12**	**20.18**	**20.31**	**20.43**	**20.89**	**20.41**	**20.31**	**20.66**	**20.62**	**20.62**
Standard deviation	**0.22**	**0.23**	**0.28**	**0.16**	**0.05**	**0.31**	**0.09**	**0.42**	**0.54**	**0.54**

Appendix D

Geometry tensile specimens

Geometry tensile specimens

12.06.2023

Dimension in mm

First batch: Stub columns

	TS-0					TS-15					TS-90			
	1	2	3	4	5	1	2	3	4	5	1	2	3	4
	7.37	7.38	7.35	7.47	7.10	7.33	7.15	7.49	7.38	7.25	7.38	7.36	7.44	7.31
Thickness	7.22	7.39	7.34	7.45	7.12	7.27	7.18	7.56	7.40	7.21	7.37	7.38	7.28	7.32
	7.23	7.43	7.31	7.59	7.16	7.23	7.18	7.42	7.44	7.29	7.37	7.39	7.26	7.29
Mean Thickness	**7.27**	**7.40**	**7.33**	**7.50**	**7.13**	**7.28**	**7.17**	**7.49**	**7.41**	**7.25**	**7.37**	**7.38**	**7.33**	**7.31**
Standard deviation	**0.08**	**0.03**	**0.02**	**0.08**	**0.03**	**0.05**	**0.02**	**0.07**	**0.03**	**0.04**	**0.01**	**0.02**	**0.10**	**0.02**
	9.58	9.31	9.53	9.59	8.59	9.77	9.83	9.64	9.79	9.62	9.66	9.59	9.59	9.61
Width	9.62	9.30	9.56	9.60	8.51	9.80	9.93	9.73	9.79	9.69	9.59	9.55	9.52	9.60
	9.58	9.17	9.53	9.55	8.92	9.79	9.82	9.76	9.71	9.85	9.67	9.55	9.71	9.71
Mean Width	**9.59**	**9.26**	**9.54**	**9.58**	**8.67**	**9.79**	**9.86**	**9.71**	**9.76**	**9.72**	**9.64**	**9.56**	**9.61**	**9.64**
Standard deviation	**0.02**	**0.08**	**0.02**	**0.03**	**0.22**	**0.02**	**0.06**	**0.06**	**0.05**	**0.12**	**0.04**	**0.02**	**0.10**	**0.06**

Second batch: Long columns

	TL-0					TL-15					TL-90			
	1	2	3	4	5	1	2	3	4	5	1	2	3	4
	8.60	8.66	8.62	8.64	8.76	8.97	8.53	8.91	8.66	8.98	8.71	8.73	8.76	8.71
Thickness	8.67	8.71	8.64	8.70	8.75	8.87	8.58	8.85	8.66	8.91	8.70	8.72	8.79	8.68
	8.79	8.69	8.65	8.74	8.82	8.91	8.61	8.80	8.70	8.86	8.73	8.72	8.77	8.63
Mean Thickness	**8.69**	**8.69**	**8.64**	**8.69**	**8.78**	**8.92**	**8.57**	**8.85**	**8.67**	**8.92**	**8.71**	**8.72**	**8.77**	**8.67**
Standard deviation	**0.10**	**0.03**	**0.02**	**0.05**	**0.04**	**0.05**	**0.04**	**0.06**	**0.02**	**0.06**	**0.02**	**0.01**	**0.02**	**0.04**
	9.87	9.66	9.83	9.82	9.85	9.91	9.69	9.77	9.91	9.84	9.90	9.92	9.90	8.74
Width	9.87	9.63	9.84	9.85	9.88	9.91	9.77	9.79	9.89	9.87	10.02	10.00	9.99	8.68
	9.92	9.70	9.90	9.87	9.87	9.99	9.74	9.72	9.89	9.94	10.08	10.01	10.00	8.69
Mean Width	**9.89**	**9.66**	**9.86**	**9.85**	**9.87**	**9.94**	**9.73**	**9.76**	**9.90**	**9.88**	**10.00**	**9.98**	**9.96**	**8.70**
Standard deviation	**0.03**	**0.04**	**0.04**	**0.03**	**0.02**	**0.05**	**0.04**	**0.04**	**0.01**	**0.05**	**0.09**	**0.05**	**0.06**	**0.03**

Appendix E

Geometry columns

Geometry columns

31.05.2023

Dimension in mm

Steel Profile					
Inner Diameter	Outer Diameter	Thickness	Steel grade	(d/t) / 90ε2	Yield Strength
75.3	82.5	3.6	S355	0.38	449

Veneer Profile	
Thickness	Glue
0.6	HB S309 PURBOND
	HB S709 PURBOND

		Measure	S-S-0	S-ST-0	S-ST-15	S-T-0	S-T-15	L-S-0	L-ST-0	L-ST-15
THICKNESS	Top Thickness	0		14.50	16.50	10.00	10.70		15.50	16.20
		90		14.20	15.20	10.10	9.60		14.70	15.10
		180		14.40	14.60	10.00	9.30		13.30	13.40
		270		10.70	16.90	10.70	10.60		13.80	14.60
	Mean Top	-		*13.45*	*15.80*	*10.20*	*10.05*		*14.33*	*14.83*
	Stand Abw.	-		*1.59*	*0.94*	*0.29*	*0.61*		*0.84*	*1.01*
	Bottom Thickness	0	3.60	14.70	16.30	10.30	10.90	3.60	15.50	17.90
		90		14.50	15.60	9.80	10.30		16.50	14.70
		180		14.30	15.70	9.60	10.40		14.90	14.10
		270		13.90	16.40	10.90	10.40		13.20	15.10
	Mean Bottom			*14.35*	*16.00*	*10.15*	*10.50*		*15.03*	*15.45*
	Stand Abw.			*0.30*	*0.35*	*0.50*	*0.23*		*1.20*	*1.46*
	Middle Section			-	-	-	-		10.60	12.10
	Mean Thickness		**3.60**	**13.90**	**15.90**	**10.18**	**10.28**	**3.60**	**14.68**	**15.14**
	Stand Abw.		**-**	***1.31***	***0.76***	***0.44***	***0.55***	**-**	***1.17***	***1.38***
INNER DIAMETER	Top Inner Diameter	0				83.80	84.00			
		90				83.30	83.80			
		180				83.60	84.00			
		270				83.80	83.80			
	Mean Bottom					*83.63*	*83.90*			
	Stand Abw.					*0.20*	*0.10*			
	Bottom Inner Diameter	0	75.30	75.30	75.30	83.70	83.70	75.30	75.30	75.30
		90				84.20	84.40			
		180				83.60	84.50			
		270				83.80	84.60			
	Mean Bottom					*83.83*	*84.30*			
	Stand Abw.					*0.23*	*0.35*			
	Mean Inner Diameter		**75.30**	**75.30**	**75.30**	**83.73**	**84.10**	**75.30**	**75.30**	**75.30**
	Stand Abw.		**-**	**-**	**-**	***0.25***	***0.35***	**-**	**-**	**-**
Outer Diameter			**82.50**	**103.10**	**107.10**	**104.15**	**104.55**	**82.50**	**104.65**	**105.58**
Length			**288.00**	**280.00**	**280.00**	**280.00**	**280.00**	**2000.00**	**2000.00**	**2000.00**

Measurament orientation

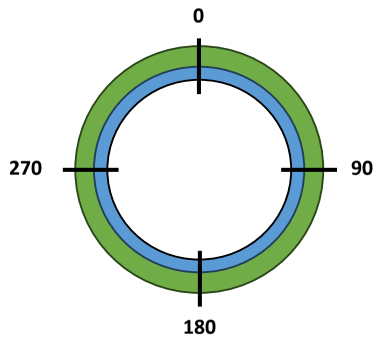

Appendix F

Steel Quadri-Linear Stress-Strain relation

Modelling steel material

15.06.2023

Parameters

f_y	449	[MPa]
f_u	547	[MPa]
E	210000	[MPa]
E_sh	3046.83	[MPa]
ε_{sh}	0.027	[-]
ε_{u}	0.107	[-]
C1	0.439	[-]
C2	0.547	[-]

$$\varepsilon_u = 0.6\left(1-\frac{f_y}{f_u}\right), \quad \text{but } \varepsilon_u \geq 0.06 \text{ for hot-rolled steels} \qquad C_1 = \frac{\varepsilon_{sh} + 0.25(\varepsilon_u - \varepsilon_{sh})}{\varepsilon_u}$$

$$\varepsilon_{sh} = 0.1\frac{f_y}{f_u} - 0.055, \quad \text{but } 0.015 \leq \varepsilon_{sh} \leq 0.03 \qquad E_{sh} = \frac{f_u - f_y}{0.4(\varepsilon_u - \varepsilon_{sh})}$$

	Engineering Stress-Strain			True Stress-Strain		
	Tot Strain	Stress	Plastic Strain	Tot Strain	Stress	Plastic Strain
	[-]	[MPa]	[-]	[-]	[MPa]	[-]
	0.000	0	0	0.0000	0.00	0.0000
ε_y	0.0021	449.00	0	0.0021	449.96	0.0000
ε_{sh}	0.0271	449.00	0.0249	0.0267	461.16	0.0246
$C_1\varepsilon_u$	0.0472	510.25	0.0450	0.0461	534.33	0.0440
ε_u	0.1075	547.00	0.1054	0.1021	605.80	0.1000
	0.1500	547.00	0.1479	0.1398	629.05	0.1376
	0.2000	100.00	0.1979	0.1823	120.00	0.1802

$$f(\varepsilon) = \begin{cases} E\varepsilon & \text{for } \varepsilon \leq \varepsilon_y \\ f_y & \text{for } \varepsilon_y < \varepsilon \leq \varepsilon_{sh} \\ f_y + E_{sh}(\varepsilon - \varepsilon_{sh}) & \text{for } \varepsilon_{sh} < \varepsilon \leq C_1\varepsilon_u \\ f_{C_1\varepsilon_u} + \dfrac{f_u - f_{C_1\varepsilon_u}}{\varepsilon_u - C_1\varepsilon_u}(\varepsilon - C_1\varepsilon_u) & \text{for } C_1\varepsilon_u < \varepsilon \leq \varepsilon_u \end{cases} \quad \text{(quad-linear model)}$$

Appendix G

Calibration timber parameters

Modelling timber veneer material

28.06.2023

Direction definition:	
1	Radial
2	Tangential
3	Longitudinal

Literature

Young's Modulus

E_1	630	MPa	
E_2	630	MPa	
E_3	12000	MPa	

Poisson ratio

v_21	0.2	v_12	0.2
v_31	0.55	v_13	0.028875
v_32	0.55	v_23	0.028875

f_R	7.9	f_TR	11
f_T	7.9	f_LR	11
f_L	71	f_LT	11
Ratio f_T/f_L	0.111		

ABAQUS Input

Elastic		
E1	630	MPa
E2	630	MPa
E3	12000	MPa
Nu12	0.2	-
Nu13	0.0289	-
Nu23	0.0289	-
G12	100	MPa
G13	720	MPa
G23	720	MPa

Plastic		
Yield Stress	71	MPa
Plastic Strain	0	-
Potential		
R11	0.1113	-
R22	0.1113	-
R33	1	-
R12	0.1549	-
R13	0.1549	-
R23	0.1549	-

Bending

Young's Modulus

E_R	1624.40	MPa		
E_b,90	1624.40	MPa		7.63770869
E_b,0	12406.70	MPa		
Ratio E_T/E_L	0.13			

Poisson ratio

v_21	0.2	v_12	0.2
v_31	0.55	v_13	0.07201113
v_32	0.55	v_23	0.07201113

f_R	14.54	f_TR	11
f_T=f_b,90	14.54	f_LR	11
f_L = f_b,0	140.47	f_LT	11
Ratio f_T/f_L	0.10		

ABAQUS Input

Elastic		
E1	1624.4	MPa
E2	1624.4	MPa
E3	12406.7	MPa
Nu12	0.2	-
Nu13	0.0720	-
Nu23	0.0720	-
G12	100	MPa
G13	720	MPa
G23	720	MPa

Plastic		
Yield Stress	140.468724	MPa
Plastic Strain	0	-
Potential		
R11	0.1035	-
R22	0.1035	-
R33	1	-
R12	0.0783	-
R13	0.0783	-
R23	0.0783	-

Tensile

Young's Modulus

E_1	2579.75	MPa		
E_2	2579.75	MPa		11.3421091
E_3	29259.82	MPa		
Ratio E_T/E_L	0.09			

Poisson ratio

v_21	0.2	v_12	0.2
v_31	0.55	v_13	0.04849186
v_32	0.55	v_23	0.04849186

f_R	11.88	f_TR	11
f_T=f_b,90	11.88	f_LR	11
f_L = f_b,0	128.26	f_LT	11
Ratio f_T/f_L	0.09		

ABAQUS Input

Elastic		
E1	2579.8	MPa
E2	2579.8	MPa
E3	29259.8	MPa
Nu12	0.2	-
Nu13	0.0485	-
Nu23	0.0485	-
G12	100	MPa
G13	720	MPa
G23	720	MPa

Plastic		
Yield Stress	128.259355	MPa
Plastic Strain	0	-
Potential		
R11	0.0926	-
R22	0.0926	-
R33	1	-
R12	0.0858	-
R13	0.0858	-
R23	0.0858	-

Compression

Young's Modulus

E_1	1234.60	MPa	
E_2	1234.60	MPa	
E_3	11269.96	MPa	
Ratio E_T/E_L	0.11	Mean between Bending and Tensile	

Poisson ratio

v_21	0.2	v_12	0.2
v_31	0.55	v_13	0.06025149
v_32	0.55	v_23	0.06025149

f_R	5.71	f_TR	11
f_T	5.71	f_LR	11
f_L = f_c,0	57.08	f_LT	11
Ratio f_T/f_L	0.10	Mean between Bending and Tensile	

ABAQUS Input

Elastic		
E1	1234.6	MPa
E2	1234.6	MPa
E3	11270.0	MPa
Nu12	0.2	-
Nu13	0.0603	-
Nu23	0.0603	-
G12	100	MPa
G13	720	MPa
G23	720	MPa

Plastic		
Yield Stress	57.0783378	MPa
Plastic Strain	0	-
Potential		
R11	0.1000	-
R22	0.1000	-
R33	1	-
R12	0.1927	-
R13	0.1927	-
R23	0.1927	-

Compression - SIA 265

Young's Modulus

E_1	1234.60	MPa	
E_2	1234.60	MPa	
E_3	11269.96	MPa	
Ratio E_T/E_L	0.11	Mean between Bending and Tensile	

Poisson ratio

v_21	0.2	v_12	0.2
v_31	0.55	v_13	0.06025149
v_32	0.55	v_23	0.06025149

f_R	1.45	f_TR	11
f_T	1.45	f_LR	11
f_L = f_c,0	57.08	f_LT	11
Ratio f_T/f_L	0.025		

ABAQUS Input

Elastic		
E1	1234.6	MPa
E2	1234.6	MPa
E3	11270.0	MPa
Nu12	0.2	-
Nu13	0.0603	-
Nu23	0.0603	-
G12	100	MPa
G13	720	MPa
G23	720	MPa

Plastic		
Yield Stress	57.0783378	MPa
Plastic Strain	0	-
Potential		
R11	0.0254	-
R22	0.0254	-
R33	1	-
R12	0.1927	-
R13	0.1927	-
R23	0.1927	-

Bibliography

[1] A. Hassanieh, H.R. Valipour, and M.A. Bradford. *Experimental and numerical study of steel-timber composite (STC) beams.* Journal of Constructional Steel Research 122 (2016) 367-378, 2016.

[2] Qiyun Qiaoa, Zhaoyuan Yanga, and Ben Mou. *Experimental study on axial compressive behavior of CFRP confined square timber filled steel tube stub columns.* Structures 24 (2020) 823-834, 2020.

[3] Hassan Karampour, Mélanie Bourges, Benoit P. Gilbert, Andrew Bismire, Henri Bailleres, and Hong Guan. *Compressive behaviour of novel timber-filled steel tubular (TFST) columns.* Construction and Building Materials 238 (2020) 117734, 2020.

[4] Tohid Ghanbari Ghazijahani, Hui Jia, and Damien Holloway. *Timber filled CFRP jacketed circular steel tubes under axial compression.* Construction and Building Materials 94 (2015) 791-799, 2015.

[5] Tohid Ghanbari-Ghazijahani, Ghazanfar Ali Magsi, Dian Gu, Amin Nabati, and Ching-Tai Ng. *Double-skin concrete-timber-filled steel columns under compression.* Engineering Structures 200 (2019) 109537, 2019.

[6] Qibin Hu, Ying Gao, Xinmiao Meng, and Yue Diao. *Axial compression of steel-timber composite column cosisting of H-shaped steel and glulam.* Engineering Structures 216 (2020) 110561, 2020.

[7] L.Kia and H. R. Valipour. *Composite timber-steel encased columns subjected to concentric loading.* Engineering Structures 232 (2021) 111825, 2021.

[8] DEUTSCHE NORM. *DIN EN 408, Holzbauwerke - Bauholz für tragende Zwecke und Brettschichtholz - Bestimmung einiger physikalischer und mechanischer Eigenschaften.* DIN EN 408, 2012.

[9] SZS Stahlbau Zentrum Schweiz. *C4/21 Bemessungstafeln.* Stahlbau Zentrum Schweiz, 2021.

[10] Xin Meng and Leroy Gardner. *Flexural buckling of normal and high strength steel CHS columns.* Structures 34 (2021) 4364-4375, 2021.

[11] Xiang Yun and Leroy Gardner. *Stress-strain curves for hot rolled steels.* Journal of Constructional Steel Research 133 (2017) 36-46, 2017.

[12] S. T. Akter, Serrano E., and Bader T. K. *Numerical modelling of wood under combined loading of compression perpendicular to the grain and rolling shear. Engineering Structures.* Engineering Structures,244, 112800, 2021.

[13] Beate Buchelt and André Wagenführ. *The mechanical behaviour of veneer subjected to bending and tensile loads.* Holz als Rohr- und Werkstoff, 66, 289-294, 2008.

[14] Robert Staudacher. *Ausgewählte mechanische Eigenschaften von Furnier der Holzarten Fichte, Birke und Buche.* Technische Universität Graz, Institut für Holzbau und Holztechnologie Granz, 2015.

[15] Technical Committee CEN/TC 250. *Eurocode 3: Design of steel structures - Part 1-14: Design assisted by finite element analysis.* prEN 1993-1-14, 2020.

[16] DEUTSCHE NORM. *Eurocode 3: Bemessung und Konstruktion von Stahlbauten - Teil 1-1: Allgemeine Bemessungsregeln und Regeln für den Hochbau; Deutsche und Englische Fassung prEN 1993-1-1:2020.* EN1993-1-1, 2020.

[17] SCHWEIZER NORMEN. *SIA 265 - Holzbau.* Schweizerischer Ingenieurund Architektenverein, Zürich, 2012.

Eidgenössische Technische Hochschule Zürich
Swiss Federal Institute of Technology Zurich

Institute of Structural Engineering (IBK)
Prof. Dr. A. Taras

Title of work:

Feasibility study and numerical investigation of novel timber veneer-wrapped steel columns

Thesis type and date:

Master Thesis, SS 2023

Supervision:

Prof. Dr. Andreas Taras,
Dr. Valentino Vigneri

Student:

Name:	Morena Giulieri
E-mail:	gmorena@student.ethz.ch
Legi-Nr.:	17-923-368
Semester:	4

Statement regarding plagiarism:

By signing this statement, I affirm that I have read and signed the Declaration of Originality, independently produced this paper, and adhered to the general practice of source citation in this subject-area.

Declaration of Originality:

`http://www.ethz.ch/faculty/exams/plagiarism/confirmation_en.pdf`

Zurich, 28. 2. 2024: _____